DIRECT DATA-DRIVEN CONTROL OF CAVITY TUNERS IN PARTICLE ACCELERATORS

RICCARDO LODDO

POLITECNICO
MILANO 1863

Master Thesis in Engineering Physics
School of Industrial and Information Engineering
Politecnico di Milano

Supervisor: Prof. Andrea Maria Zanchettin
Co-Supervisor: Prof. Simone Formentin
Co-Supervisor: Dr. Rocco Paparella

Student ID: 850603

September 2017

ABSTRACT

X-Ray Free Electron Lasers (XFELs) are the next generation of X-rays sources delivering dramatical improvements over synchrotron radiation in terms of brilliance, pulse length and coherence. The laser-like properties of XFEL radiation allow experiments not possible before in numerous research fields such as plasma physics, condensed matter physics, material science, femtochemistry and structural biology. To obtain the X-ray radiation, accelerated electronic beams are propagated in undulators, where X-rays are emitted according to a Self-Amplified Spontaneous Emission (SASE) process. The high gradients of the accelerating electromagnetic field, external vibrations and pressure fluctuations cause deformations of the cavities where the electrons are accelerated. This lowers the efficiency of the Linear Accelerator (LINAC) and degrades the beam quality. To contrast this phenomenon, indicated with the term *detuning*, tuners capable of mechanical compensation of cavity deformations have been developed and successfully employed in LINACs.
In the present work we look at the challenges in the control of these tuners during cavity operations, and we propose an offline data-driven approach for the synthesis of the controllers. This approach is presented as an alternative to the on-line iterative methods currently in use. Iterative methods, by adjusting the controller parameters during operation, are able to respond to shifts of the system parameters but the obtained controlled system is nonlinear and its convergence to a stable system depends on manually tuned parameters. The direct offline methods proposed, the Virtual Reference Feedback Tuning (VRFT) and the Correlation Approach, offer instead an overall linear device free of convergence issues. These methods are tested on a simulated system and their performance are discussed in presence of noise.

SOMMARIO

I laser ad elettroni liberi nei raggi X (XFELs) rappresentano una nuova generazione di sorgenti di radiazione, capace di fornire miglioramenti rispetto alla radiazione di sincrotrone sia in termini di brillanza sia in termini di coerenza e durata temporale dell'impulso. Le proprietà della radiazione da sorgenti XFEL consentono esperimenti prima non realizzabili in numerosi campi di ricerca. Applicazioni sono state proposte in fisica dei plasmi, fisica della materia condensata, scienza dei materiali, femtochimica, biologia strutturale e altri numerosi campi. La generazione di radiazione nei raggi X sfrutta un processo di emissione spontanea auto amplificata (SASE) da parte di fasci elettronici propaganti in un undulatore. Gli elettroni sono precedentemente accelerati in un acceleratore lineare (LINAC) dove il forte campo elettromagnetico accelerante, vibrazioni esterne e fluttuazioni di pressione causano deformazioni nelle cavità risonanti dell'acceleratore stesso. Queste deformazioni causano un abbassamento dell'efficienza e una degradazione della qualità del fascio. Per contrastare questo fenomeno, indicato con il termine *detuning*, sono stati sviluppati dispositivi capaci di compensare meccanicamente le deformazioni delle cavità dell'acceleratore durante il suo funzionamento.
In questo lavoro verranno discusse le difficoltà nel controllo di questi dispositivi, proponendo un approccio data-driven e offline per la sintesi di un sistema di controllo capace di compensare il detuning. Nei LINAC attualmente in operazione sono impiegati metodi diretti iterativi. Questi metodi, aggiornando i parametri di controllo durante il funzionamento dell'acceleratore, sono in grado di rispondere a cambiamenti del sistema ma forniscono un dispositivo di controllo complessivamente non lineare la cui stabilità e capacità nel convergere a un sistema stabile dipende da parametri scelti manualmente. I metodi offline proposti, il Virtual Reference Feedback Tuning (VRFT) e l'Approccio a Correlazione, mantengono la linearità del sistema e sono privi di iterazioni, perciò privi di problemi legati alla convergenza. Il controllore è direttamente sintetizzato da dati provenienti da esperimenti ingresso/uscita, senza il passo intermedio di stima del modello del sistema da controllare che caratterizza le tecniche Model Based, ottenedo una soluzione al problema del controllo definita *one-shot*.
Questi metodi verranno testati su un sistema simulato verificandone le prestazioni in presenza di rumore.

ACKNOWLEDGEMENTS

I would like to thank my supervisors prof. Andrea Zanchettin and prof. Simone Formentin for the opportunity to work at this thesis and their support during these months.
Grateful thanks to Rocco Paparella, Istituto Nazionale di Fisica Nucleare (INFN) Laboratorio Acceleratori e Superconduttività Applicata (LASA) (Milano, Italy), for making this thesis possible in the first place and his support during these months.
Special thanks to my family for their assistance and encouragement during all these years in my educational path.

CONTENTS

LIST OF FIGURES

LIST OF TABLES

1 INTRODUCTION

X-Ray radiation has long been proven to be a versatile tool in many research fields. Discovered at the end of the 19th century by Wilhelm Conrad Roentgen, it has found immediate application in medicine starting the field of diagnostic radiography. The study of X-rays diffraction by Max von Laue, awarderd a Nobel prize in physics, opened the study of the structure of crystals, notably including crystals obtained from organic molecules. The analysis of the structure of proteins, viruses and the DNA was made possible by X-ray radiation [11]. The increasing popularity of X-rays has led to a continuous development of radiation sources satisfying the increasing needs of the scientific community. Until a decade ago the state of the art of X-rays was represented by synchrotron radiation, obtained by electrons accelerated in a storage ring configuration. The inability of these radiation sources to fulfill increasing research requirements either in terms of average brilliance, pulse length, coherence or collimation has led the development of a new generation of X-ray sources representing an evolutionary improvement. X-Ray Free Electron Lasers (XFELs), based on the Self Amplified Spontaneous Emission (SASE)[1] principle, were constructed to produce X-ray radiation with laser light properties.

The Free Electron Laser in Hamburg (FLASH) is the first operating FEL facility, delivering, in the soft X-rays, an increase of more than 8 orders of magnitude in peak brilliance compared to the state of the art of synchrotron radiation such as the one emitted by the BESSY II, operated by the Berlin Electron Storage Ring Society for Synchrotron Radiation, and the Swiss Synchrotron Light Source SLS. The Linac Coherent Light Source (LCLS) is the first operating FEL source in the hard X-Rays delivering similar improvements over the European Synchrotron Radiation Facility. The European XFEL currently represents the state of the art in the generation of hard X-rays, targeting pulse durations shorter then 100 fs (compared to 100 ps for the ESRF) and peak brilliance in the order of 10^{33} photons/s $\cdot$ mm^2 $\cdot$ mrad^2 $\cdot$ 0.1%BW (compared to 10^{24} for the ESRF). In light of this improvements FEL are considered the fourth generation of X-Ray sources, offering dra-

1 A linearly accelerated electronic beam is propagated in an undulator. An electron, interacting with the undulator's sinusoidally modulated magnetic field, emits an electromagnetic wave-train with a wavelength function of its energy and the undulator's period. In a beam the electrons do not only interact with the modulated magnetic field but also with each other. The combined interaction leads to a spatial distribution of the electrons along the propagating axis at a wavelength apart, emitting an in-phase wave-train with the properties of laser radiation [18].

matical improvements over synchrotron radiation making possible new applications of X-ray radiation.
The availability of femtoseconds X-ray pulses makes possible, via diffraction, the study of the structure and dynamics of molecules and clusters as well as the study of electron dynamics of X-ray irradiated targets. The pulse duration is comparable with the dynamics of molecular bonds making possible structural studies of chemical process in the femtoseconds range including pump-probe experiments with femtoseconds pulses, leading to new advancement in femtochemistry. In plasma physics XFEL radiation allows to reach new plasma states at higher temperatures and pressures than before, new studies of the interaction between X-rays and plasmas, and makes possible advancements in plasma spectroscopy. In condensed matter physics it is posed to become an important tool in the investigation of open problems in magnetism and phase transitions. Its qualities are expected to make possible the study by diffraction of organic molecules that cannot be process into crystal making it a valuable tool in structural biology. Many more applications are expected to surface involving this new radiation source, making XFELs a new important tool in scientific research[23].

1.1 LINEAR ACCELERATORS IN XFELS

The basic of operation of the European XFEL can be described by starting from the generation of the electron bunches used to emit X-ray radiation[1]. A solid cathode is irradiated by a laser beam and the extracted electrons are accelerated by a Radio Frequency (RF) gun towards a Linear Accelerator (LINAC). After multiple stages of acceleration and bunch compression the electrons reach the undulators where the X-ray radiation is generated according to the SASE principle and then sent to experimental stations. The electrons are instead discarded in beam dumps.
The LINAC stage is based on the technology of the Tera-Electronvolt Superconducting Linear Accelerator (TESLA) Test Facility (TTF), originally developed for the use in a linear collider. The electronic beams travels in nine-cell Niobium cavities where are accelerated by a resonating electromagnetic field. Each cavity is tuned for operation for the TM_{010} π-mode[2] at 1.3 GHz, and operated in cryostat modules, maintaining the cryogenic temperatures required for Niobium superconductivity. The LINAC stage includes a total of 808 cavities (101 cryomodules), divided in 26 RF stations for a length of 1.6 km to bring the electrons received from the RF gun from 120 MeV to 17.5

2 On the symmetry axis of the cavity the electric field oscillates as a standing wave with a node between each cell. The travelling beam interacting with the field receives an on-crest acceleration proportional to the field oscillation amplitude.

GeV. A pulsed operation is targeted with a 10 Hz repetition rate for the acceleration of a maximum pulse length of 800 μ and an electronic current of 4.5 mA.

1.2 DETUNING

To deliver the required beam quality and to keep the accelerating process efficient the frequency of the TM_{010} π-mode of the cavities should remain as close as possible to its nominal value. During operation electromagnetic pressure on the internal cavity walls leads to time-varying deformations capable of pushing the resonant frequency outside tolerable limits when high accelerating gradients (> 25 MV/m) are involved. Vibrations from the external environments, fluctuation of helium pressure are some of the external factors that contributes to a change in the resonant frequency of the accelerating electromagnetic mode of the cavity. Detuning, the shift of the resonant frequency from its nominal value, has required the development of tuning systems capable of dynamic mechanical compensation of cavity deformations by regulating the cavity length.
In the European XFEL each cavity is equipped with a tuner based on the Saclay I design, developed by the French Alternative Energies and Atomic Energy Commission (CEA) research center in Saclay and later modified by the German Electrosynchrotron (DESY) research center. This tuning system includes a double stack piezo configuration (one as a sensor, the other as an actuator) to provide the dynamic mechanical compensation of detuning.

1.3 CONTROL METHODS

One of the challenges represented by the tuning system is the control of the piezoelectric actuator during operation. Complex mechanical coupling of the actuator to the cavity leads to a wealth of resonances and antiresonances preventing the use of schemes based exclusively on feedback control. Simple Proportional Integral Derivative (PID) controllers are unable to produce stable closed loop system with sufficient speed for the compensation of the dynamic detuning from Lorentz forces. Model based control designs, such as the Kalman filter or Model Predictive Control (MPC), needs an intermediate step where a model of the system is be estimated. Uncertainties in the experimentally estimated model can impact negatively the performance of the controlled system and variations between different cavities require a different estimated model for each tuner-cavity installation (808 in the XFEL). Indirect self-tuning system, where an estimation of the system is calculated online, have been considered impractical due to the high computational costs of their DSP or FPGA implemen-

tation. Furthermore the closed loop update of the system estimate makes such controllers nonlinear systems, making even stability requirements hard to assure in non-specific cases.
Direct schemes that include, or use exclusively, feedforward action have instead been successfully implemented and are currently in use in FELs. In contrast with indirect methods the intermediate step of estimation of the plant model is avoided and the controller or feedforward filter parameters are obtained minimizing a cost function depending explicitly only on input/output data. The piezoelectric actuator in the European XFEL is driven according to a feedforward scheme in which the filter is synthesized using an direct iterative control method. At each iteration, consisting in the 1.4 ms XFEL pulse, the cavity detuning is collected and used to update the filter coefficients [21][20].
Continuous Wave (CW) operation of XFELs (currently a proposed extension for the European XFEL[6]) is particularly affected by low frequency (below 100 Hz) detuning contribution from external vibrations and pressure variations. For their compensation the use of an approach combining feedback and feedforward actions was shown effective. A manually tuned PID controller was combined with a self-tuning feedforward filter and tested at the Horizontal bi-cavity testing facility (HoBiCaT) at the Helmoholtz-Zentrum center in Berlin (HZB), reaching the piezoelectric resolution limits [17].
One drawback of iterative methods is the complexity hidden in the iterative process. The self-tuning feedforward filter tested in HoBiCaT is a non linear device that needs manual tuning of the iteration parameters to remain in a stable range. The initial conditions of the iterative process also affect its ability to converge to a filter capable of achieving compensation. The iterative feedforward algorithm in use at the European XFEL as presented in [21] is limited to the correction of the controller gain with a manually set iteration coefficient, potentially incurring in slow convergence or instability problems where to change the characteristics of the RF pulse in the accelerating cavity. Having the iterative process limited to the gain means that the time delay of the correcting pulse to sent to the piezo must be found separately. In [20] the delay is obtained by scanning over a possible range of time intervals searching for a local minimum of the detuning, an additional procedure in the feedforward filter synthesis.

1.4 OUTLINE OF THE THESIS

An application of *non-iterative* direct methods is proposed for the synthesis of a feedback controller and a feedforward filter with the intention to provide an alternative free of manually tuned parameters, reducing the implementation burden, and capable of synthesizing the controller using only input/output data from the cavity in operation with no intermediate step of model estimation. Such methods have been called *one-shot* for their ability to return a controller from a single experiment and no intermediate steps.
Before their introduction a quantitative description of the effects of detuning on the acceleration of the electronic beam is given in Chapter 2. A model for the main cause of detuning, the electromagnetic pressure acting on the cavity walls, is presented, while the detuning effects of external vibrations and pressure of the helium bath are treated as a stochastic disturbance.
To compensate the cavity detuning different devices have been developed, and a brief overview is given in Chapter 3. Mechanical tuners are able to compensate the detuning by a mechanical deformation of the cavity even during operation by employing piezoelectric actuators and sensors. The mechanical coupling of the actuator to the cavity leads to a frequency response rich with resonances and anti-resonances constituting a challenge for control. In Chapter 4 the proposed control scheme for the compensation of detuning by the mechanical tuners is introduced. The Virtual Reference Feedback Tuning (VRFT) [7] and the Correlation Approach [12] are chosen to be applied to the synthesis of a feedback controller and a feedforward filter, to obtain a fully offline direct non-iterative design method for the compensation of detuning in both CW and pulsed cavity operation.
Finally the obtained approach to detuning compensation is put to the test on a simulated system in Chapter 5, both in pulsed and continuous wave operation, with concluding remarks in Chapter 6.

2

DETUNING

The TESLA cavity is designed to have the beam accelerating resonant mode of the electromagnetic field at the fixed frequency of 1.3 GHz. Electromagnetic pressure inside the cavity , mechanical vibrations and pressure fluctuation of the helium bath are the leading cause of shift of the resonant frequency via mechanical deformations of its walls. This phenomenon, indicated with the term *detuning*, causes a decrease of the effective accelerating gradient and a deterioration of the beam quality possibly leading the requirements for a pure RF compensation outside tolerable limits. In pulsed operation electromagnetic pressure is the dominant factor in the overall cavity detuning. The high gradients (25-35 MV/m) of the RF field reached in the European XFEL during the acceleration of the electronic beam can lead to to a reduction of the accelerating voltage up to 50% , if left uncompensated. In the continuous wave operation most of the detuning contribution from electromagnetic pressure reduces to a constant term that can be compensated easily, leaving external sources as major contributors.
In this chapter the effects of detuning will be discussed quantitatively using an RLC model of the cavity, giving particular attention the resulting loss of accelerating voltage. A model for the effects of electromagnetic pressure on the cavity, the dominant cause of detuning, will be presented, while the overall effect of the external causes of detuning of the cavity will be treated as a stochastic disturbance on the frequencies of the electromagnetic modes.

2.1 EFFECTS ON CAVITY OPERATION

The TESLA cavity is a metallic structure composed by nine cells in which an electromagnetic field from a klystron is injected. The beam of charged particles propagates along the symmetry axis and is accelerated by the electric field of a TM mode of the cavity. Along the symmetry axis, the electric field of the mode used during acceleration can be described as a standing wave with a node between each cell.
To efficiently maintain the oscillating electric field, the cavity is designed in such a way to have a resonance for the previous electromagnetic mode at the same frequency of the klystron.
An RLC model for the cavity can be employed to describe the effects of the cavity resonance on the accelerating voltage. The nine cell structure produces nine resonances for the TM_{010} mode of the cavity,

each corresponding for the electric field along the symmetry axis to a standing wave from 0 to 8 nodes between the cells. This corresponds to 9 coupled RCL circuits, as shown in figure (1).

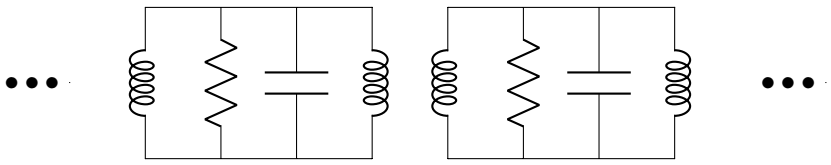

Figure 1: Multicell RLC Model of the cavity

Circuit composed by coupled RLC resonators modeling the resonant frequencies of the cavity. A more complete model includes the klystron and the transmission line.

Mode	f_m
$f_{\frac{1}{9}\pi}$	1274.387 MHz
$f_{\frac{2}{9}\pi}$	1276.435 MHz
$f_{\frac{3}{9}\pi}$	1280.206 MHz
$f_{\frac{4}{9}\pi}$	1284.409 MHz
$f_{\frac{5}{9}\pi}$	1289.022 MHz
$f_{\frac{6}{9}\pi}$	1293.345 MHz
$f_{\frac{7}{9}\pi}$	1296.861 MHz
$f_{\frac{8}{9}\pi}$	1299.260 MHz
f_{π}	1300.091 MHz

Table 1: Frequencies of the first pass-band modes of a typical TESLA cavity.

Before operation the cavity π is tuned to 1300 MHz. The relative closedness of the $\frac{8}{9}\pi$ mode to the π mode, allows it to influence the stability of the electromagnetic field during operation.

Since only the π-mode is used for beam acceleration due to higher efficiency between the accelerating voltage and the injected power required, only one resonance needs to be modeled reducing the system to a single RLC oscillator driven by the klystron through a transmission line. For the purpose of studying the behaviour of the cavity the model can be further simplified by considering the klystron as a current source and the transmission line as additional impedance. The resulting circuit is shown in figure (2).

By construction V_c is the resulting accelerating voltage of the cavity. Other parameters of the RLC circuit can also be related to measurable characteristics of the cavity.

The resonant frequency can be immediately introduced (1).

$$\omega_0 = \frac{1}{\sqrt{LC}} \tag{1}$$

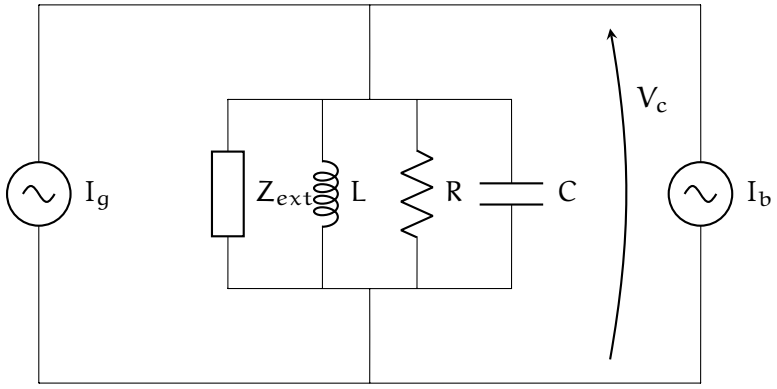

Figure 2: RLC model of the cavity for the π mode.
I_g and I_b are the currents representing the klystron and the beam respectively.

Parameter	Typical Value
ω_0	1.3GHz
β	3000
Q_L	$3.6 \cdot 10^6$
$\omega_{1/2}$	200Hz
R_L	1.55GΩ

Table 2: Typical characteristics for the TESLA cavity.
ω_0 is the natural frequency of the resonance used for beam acceleration, β is the ratio of external and internal dissipated power during operation, Q_L is the quality factor, $\omega_{1/2}$ is the bandwidth of π-mode, R_L is the total shunt resistance.

For the quality factor of the resonant mode we first distinguish between the power dissipated in the cavity and external dissipated power, for example due to losses within the transmission line. In particular to avoid damages to the klystorn due to reflected RF waves a circulator with a matched load Z_0 is located between it and the cavity resulting in an additional dissipative term for the RLC circuit.

$$Q_0 = \frac{\omega_0 W}{P_{diss,cav}} = \omega_0 RC = \frac{R}{L\omega_0} \tag{2}$$

$$Q_{ext} = \frac{\omega_0 W}{P_{diss,ext}} = \omega_0 n^2 Z_0 C \tag{3}$$

The β coefficient, the ratio between the power dissipated externally and internally to the cavity, can now be introduced:

$$\beta = \frac{P_{diss,ext}}{P_{diss,cav}} = \frac{Q_0}{Q_{ext}} = \frac{R}{n^2 Z_0} \tag{4}$$

For superconductive cavities most losses are external, for the TESLA typically $\beta > 10^3$. The effective Q factor is given by:

$$Q_L = \frac{Q_0}{1+\beta} \tag{5}$$

The cavity bandwith can be introduced from Q_L:

$$\omega_{1/2} = \frac{\omega_0}{2Q_L} = \frac{1}{\tau} \tag{6}$$

The last quantity that needs to be introduced is the shunt impedance, that can be defined as the ratio between the accelerating field amplitude and the dissipated RF power on the cavity walls (7) usually given normalized by the quality factor (8).

$$r = \int_0^L \frac{E_z^2(z)}{-dP/dz} dz \tag{7}$$

$$R = \frac{1}{2} r = \frac{1}{2}(r/Q)Q_0 \tag{8}$$

The effective load driven by the Klystron is given by the parallel of the cavity load, given by R, and the matched impedance Z_0 of the transmission line.

$$n = \sqrt{\frac{R}{\beta Z_0}} \tag{9}$$

$$R_L = R//(n^2 Z_0) = \frac{R}{1+\beta} = \frac{1}{2}(r/Q)Q_L \tag{10}$$

The previous circuit in figure (2) corresponds to the equation of the damped harmonic oscillator driven by the sum of the klystron current and the beam current:

$$\frac{d^2V_c}{dt^2} + \frac{1}{R_L C}\frac{dV_c}{dt} + \frac{1}{LC}V_c = \frac{1}{C}\frac{dI}{dt} \tag{11}$$

Using the relationships between the model parameters and the physical quantities describing the cavity the latter can be substituted obtaining:

$$\frac{d^2V}{dt^2} + 2\omega_{1/2}\frac{dV}{dt} + \omega_0^2 V = 2\omega_{1/2} R_L \frac{dI}{dt} \tag{12}$$

Equation (12) describes the behaviour of the accelerating voltage inside the cavity. To find an explicit solution the cavity will be considered in its steady-state, where the klystron current is a sinusoidal signal oscillating at its fixed frequency of 1.3 GHz and no beam are travelling along the cavity.
The Klystron current can be written as a phasor, ideally oscillating at

frequency ω_0, but in practice it differs from the cavity frequency and so it will be indicated with ω.

$$\tilde{I}(\omega, t) = I_0 e^{-j\omega t} \tag{13}$$

Since the system is linear the steady-state solution for the accelerating voltage can be written in the form:

$$\tilde{V}(\omega, t) = V_0 e^{-j\omega t} \tag{14}$$

The steady-state solutions can be substituted in equation (12) obtaining:

$$-\omega^2\tilde{V} - 2j\omega_{1/2}\omega\tilde{V} + \omega_0^2\tilde{V} = 2j\omega_{1/2}R_L\omega\tilde{I} \tag{15}$$

Which can immediately be solved by grouping $\tilde{V}$ on the left side of the expression:

$$\tilde{V} = \frac{\omega_{1/2}R_L}{\omega_{1/2} - j\frac{\omega}{2} + j\frac{\omega_0^2}{2\omega}}\tilde{I} \tag{16}$$

Ideally the cavity resonant frequency ω_0 is going to be equal to the frequency of the driving klystron ω, in practice $\omega - \omega_0 << \omega_0$, so that the solution found can be approximated:

$$\tilde{V} = \frac{\omega_{1/2}R_L}{\omega_{1/2} - j\frac{\omega^2 - \omega_0^2}{2\omega}}\tilde{I} \tag{17}$$

$$\tilde{V} = \frac{\omega_{1/2}R_L}{\omega_{1/2} - j\frac{(\omega+\omega_0)(\omega-\omega_0)}{2\omega}}\tilde{I} \approx \frac{\omega_{1/2}R_L}{\omega_{1/2} - j\frac{2\omega(\omega-\omega_0)}{2\omega}}\tilde{I} \tag{18}$$

$$\tilde{V} = \frac{\omega_{1/2}R_L}{\omega_{1/2} - j\Delta\omega}\tilde{I} \tag{19}$$

The introduced term $\Delta\omega$ is called cavity *detuning*, and represent the difference between the frequency the cavity is being operated (ω) and its resonant frequency ω_0. ω is fixed by the klystron and therefore detuning is caused by variations of the cavity resonant frequency from the desired value.

From the solution (19), written in phasor notation, follows that the cavity detuning affects both the amplitude and the phase of the accelerating voltage.

$$|V_c| = \frac{\omega_{1/2}R_L}{\sqrt{\omega_{1/2}^2 + \Delta\omega^2}} \tag{20}$$

$$\phi = tan^{-1}\frac{\Delta\omega}{\omega_{1/2}} \tag{21}$$

The immediate results of detuning is a decrease of the accelerating voltage due to a shift of the cavity resonant frequency away from the frequency where the klystron is operating. The Low Level Radio Frequency (LLRF) control system, responsible for the control of the resonating RF field with a combination of feedforward and feedback

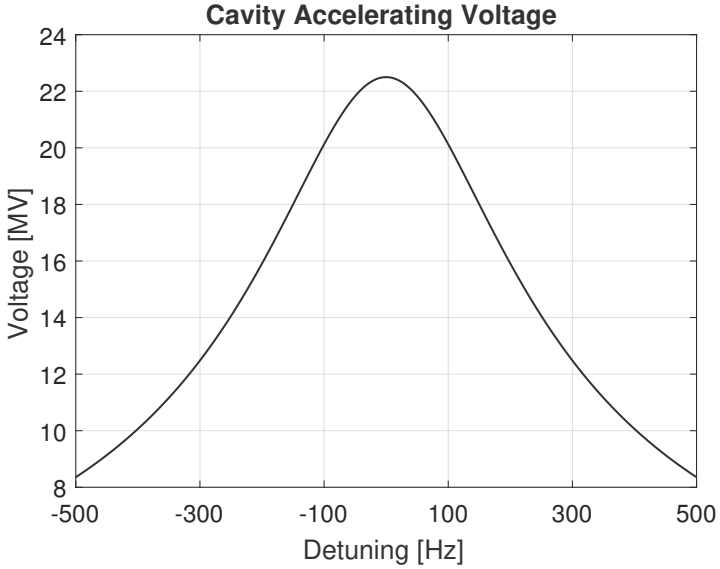

Figure 3: Detuning effects on cavity accelerating voltage

Effects on the accelerating voltage due to cavity detuning for values of typical pulsed mode operation of the TESLA cavity. ($\omega_{1/2} = 200\text{Hz}, R_L = 1.5\text{G}\Omega, I = 15\text{m}A$)

action, can compensate this effect by increasing the klystron driving current and thus the injected power into the cavity. The increased power required to maintain the amplitude of the resonating electric field to the desired point is considered as a power loss due to the presence of detuning.
To consider the effects of the phase shift we consider a small beam travelling along the symmetry axis of the cavity. In each cell the beam receives an acceleration by the resonating electric field of the cavity:

$$\Delta E = q\Delta V_{cell} \tag{22}$$

The π-mode of the cavity along the axis has only the electric component oscillating as a standing wave. By construction each cell has length $\lambda/2$:

$$\Delta E = q\int_0^{\lambda/2} E(z,t)dz = q\int_0^{\lambda/2} E_0 sin\left(\frac{2\pi}{\lambda}z\right) sin\left(\omega t(z)+\phi\right) dz \tag{23}$$

ϕ is the phase term due to detuning of the cavity. By approximating the speed of the beam with c:

$$\Delta E = q\int_0^{\lambda/2} E_0 sin\left(\frac{2\pi}{\lambda}z\right) sin\left(\frac{2\pi}{\lambda}z+\phi\right) dz \tag{24}$$

The integral can be explicitly solved:

$$\Delta E = q\int_0^{\pi} E_0 sin(u)sin(u+\phi)du = \Delta E_0 cos(\phi) \tag{25}$$

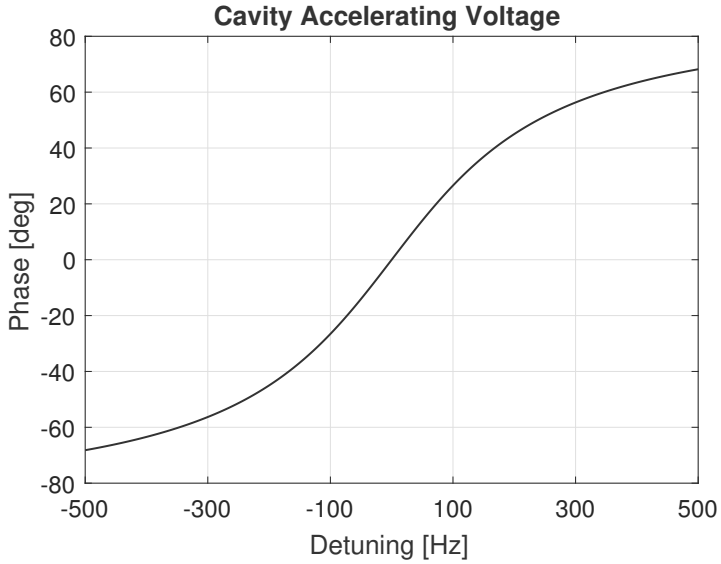

Figure 4: Cavity phase shift from detuning

Phase shift of the accelerating voltage due to cavity detuning for values of typical pulsed mode operation of the TESLA cavity. ($\omega_{1/2} = 200\text{Hz}, R_L = 1.5\text{G}\Omega, I = 15\text{m}A$)

From (25) it follows that the phase shift of the cavity causes a decrease of the *effective* accelerating voltage on top of the reduction of the actual cavity voltage as seen in (20). When the detuning is not present ΔE is maximum. This condition is called on-crest acceleration since the beam reaches the half-cavity length at the instant in which the electric field is at its peak.

An exponential term can be added to the steady-state solution by recognizing the time constant from (12) obtaining the step response of the cavity in case of static detuning.

$$\tilde{V}(\omega, t) = \frac{\omega_{1/2} R_L}{\omega_{1/2} - j\Delta\omega} \left(1 - e^{-(\omega_{1/2} - j\Delta\omega)t}\right) \tilde{I} \tag{26}$$

Detuning is caused by variation of the resonant frequency ω_0 of the cavity respect to the frequency of the driving klystron. In order to explicitly solve (12) it was considered a purely static term. During operation the cavity is exposed to static and dynamic detuning. In the following sections the most important causes of internal and external detuning will be introduced.

2.2 MICROPHONIC DETUNING

During operation, the cavity is susceptible to external mechanical disturbances: variations in pressure of the helium bath, vibrations from nearby machinery, such as helium or vacuum pumps, ground motion. The overall effect on the resonating frequency of the cavity by all the external noise sources is indicated with the term microphonic detun-

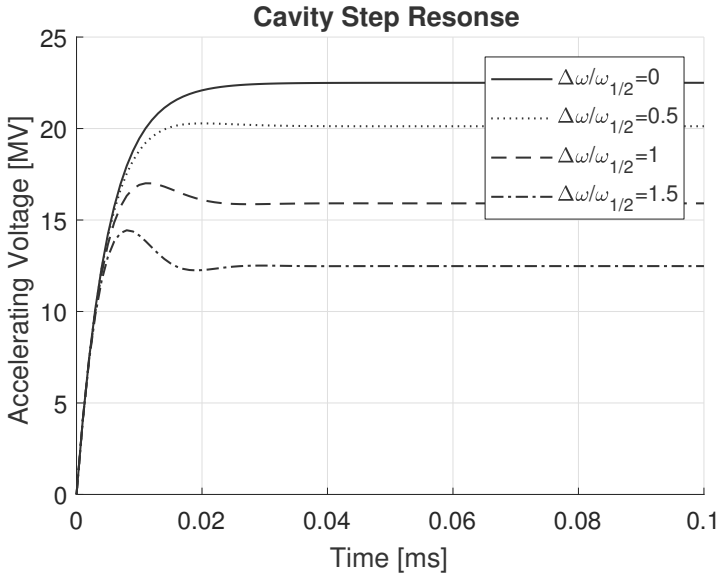

Figure 5: Step response of the cavity.

Step response of the cavity at constant detuning for various detuning values. Uncompensated detuning in the European XFEL corresponds to $\Delta\omega/\omega_{1/2} = 2$ corresponding to an increased RF power to mainting the set accelerating voltage of a factor of 2.

ing. External vibrations transmitted to the cavity cause variation of the cavity size in the order of nanometres, enough to cause detuning in the order of hertz. Due to the nature of microphonic effects there are no theoretical models available to predict the spectral properties of the disturbance on the cavity detuning from the helium bath and the external machinery. In practice in each combination of cavity and external environment the contributions of microphonics to the cavity resonant frequency will be a non-stationary non-white noise. Nevertheless it can be show by comparing different samples of microphonic detuning from different experimental setups that there are important similarities that can be exploited to produce parameters for the synthesis of a feedback controller that remain valid independently from the specific setup.
Samples of cavity detuning can be collected from the cavity in continuous wave operation using the same RF detector used in the LLRF control system. From the measured phase shift the detuning can be obtained from (21).

In general there are two main shared spectral features of the microphonic detuning [13]:

- A low frequency background from circa 0.01 Hz up to 5 Hz
- Sharp resonances between 10 Hz to 200 Hz

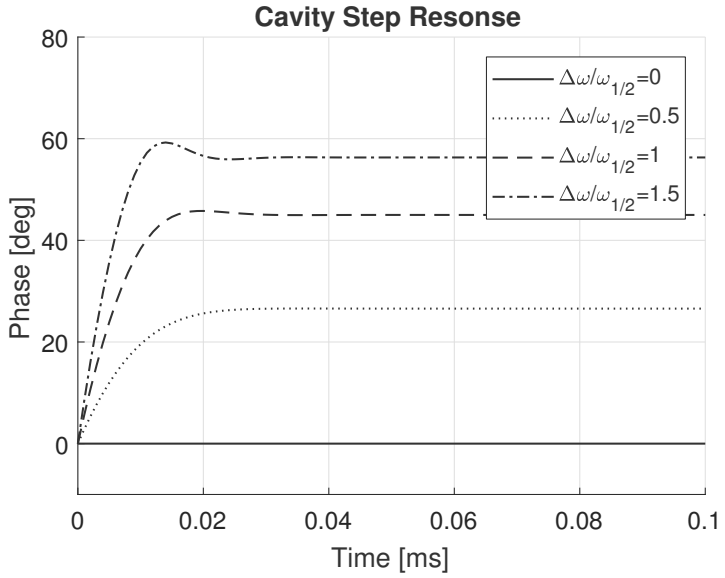

Figure 6: Phase step response of the cavity.

Phase term of the cavity step response at constant detuning. Uncompensated detuning in the European XFEL corresponds to $\Delta\omega/\omega_{1/2} = 2$ corresponding to a phase shift during beam acceleration of approximately 45 degrees.

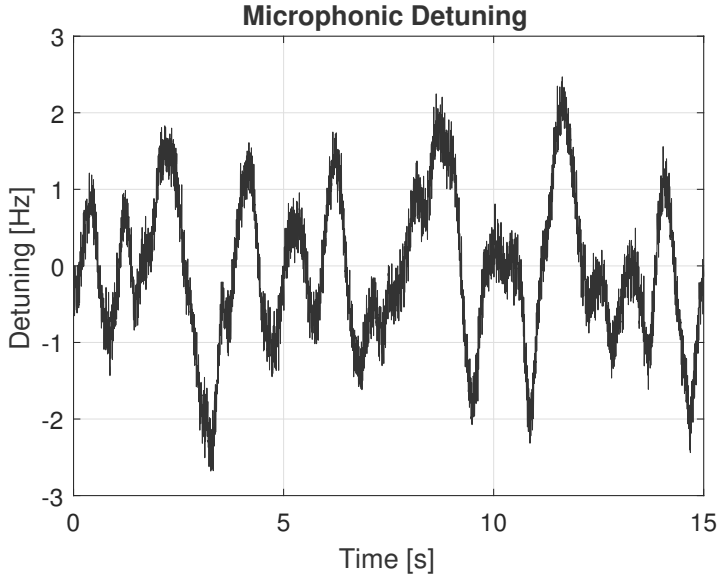

Figure 7: Simulated microphonic detuning.

The ratio of the spectral power of the low frequency background and the resonances does not depend solely the specific tuner-cavity-tank system, but it varies in time in a stochastic manner during normal operation. The main causes of the microphonics detuning remains largely the same instead: pressure fluctuation of the helium bath of the cryogenic unit, vibrations from auxiliary machinery such as vacuum pumps. To include the effects of detuning in the cavity

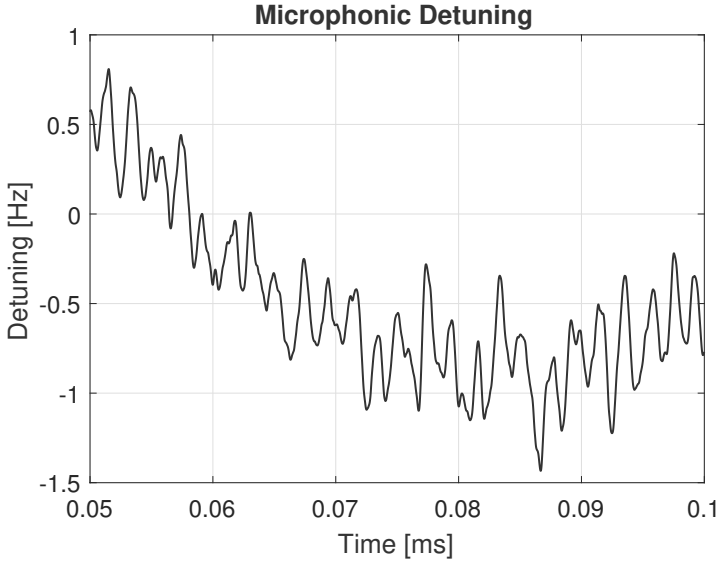

Figure 8: Simulated microphonic detuning.

Simulated microphonic detuning over a smaller time interval, oscillations from external machinery are visible.

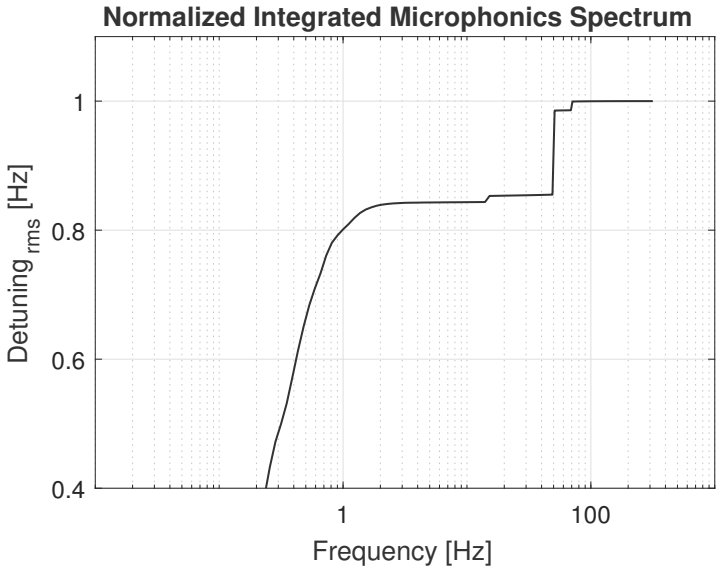

Figure 9: Simulated integrated microphonic spectra.

model a simulated detuning disturbance is superimposed to the detuning caused by Lorentz forces. The low frequency background has been reproduced by feeding a band-pass linear system white noise, while the resonance peaks from the nearby operating machinery are included by superimposing sinusoidally oscillating signals at fixed frequencies. The obtained stationary noise renders the qualitative features of experimental microphonic spectra when sampled for a sufficiently long time.

2.3 LORENTZ DETUNING

Another source of cavity detuning is the accelerating electromagnetic field itself. During operation small currents are induced on the internal layer of the metallic structure. The resonating electromagnetic field, responsible for these superficial currents, exercises a Lorentz force on them. The result is an uneven pressure on the internal cavity walls leading a deformation of the cavity.

$$p = \frac{1}{4}\left(\mu_0 H^2 - \epsilon_0 E^2\right) \tag{27}$$

The pressure from the electromagnetic field (27) is sufficient to obtain a significant variation of the internal volume of the cavity witch leads to detuning of the oscillating mode used for beam acceleration (28).

$$\frac{\Delta\omega}{\omega_0} = \frac{1}{4W}\int_{\Delta V}\left(\epsilon_0 E^2 - \mu_0 H^2\right) dV \tag{28}$$

$$W = \frac{1}{4}\int_{V}\left(\epsilon_0 E^2 + \mu_0 H^2\right) dV \tag{29}$$

The above expressions lead to a linear dependence of the detuning from the intensity of the accelerating RF field. The proportionality constant can be determined experimentally. A typical value for the static detuning of TESLA cavities is 1 $Hz/(MV/m)^2$[14]. During typical pulsed operation a value of 0.5 $Hz/(MV/m)^2$ is observed during flat-top.

(30).

$$\Delta\omega_c = -KE_{acc}^2 \tag{30}$$

For the XFEL operating at an accelerating gradient of 25 MV/m a detuning of 350 Hz can be observed, which is greater then the bandwidth cavities are typically operated at (100 - 300 Hz).

$$P_g = P_0\left(1 + \left(\frac{\Delta\omega}{\omega_{1/2}}\right)^2\right) \tag{31}$$

The additional power injected into the cavity to maintain the required effective accelerating voltage increase quadratically with the detuning (31), and the detuning from Lorentz forces increases quadratically with the accelerating voltage (30). Under these conditions the additional power required at high accelerating gradients could be substantial.

Compensating mechanically the volume change induced by the Lorentz forces allows maintaining the detuning inside the cavity bandwidth. In continuous wave operation the main contribution of Lorentz detuning is a static term (fluctuations of the amplitude of the oscillating field can give origin to a small dynamic component), that can be compensated by a pre-detuning of the cavity such that the sum of the two

contributions will cancel each other.
In pulsed operation the dynamic behaviour of Lorentz detuning cannot be neglected. The bandwidth of the variations of the amplitude of the electromagnetic field during a pulse (1.3 ms in the European XFEL) are sufficient to excite the mechanical modes of the cavity leading to an oscillating behaviour of the detuning. Since the oscillation from the mechanical modes are deterministic, the knowledge of their dynamics allows their compensation using a feedforward scheme. In general the effect of Lorentz forces on the detuning of a superconductive cavity can be described using a system of independent resonating modes, each corresponding to a cavity mechanical mode and modeled using a second order linear system.

$$\frac{d}{dt}\begin{bmatrix}\Delta\omega_m\\ \Delta\dot{\omega_m}\end{bmatrix} = \begin{bmatrix}0 & 1\\ -\omega_m^2 & -\omega_m/Q_m\end{bmatrix}\begin{bmatrix}\Delta\omega_m\\ \Delta\dot{\omega_m}\end{bmatrix} + 2\pi V_{acc}^2\begin{bmatrix}0\\ -K_m\omega_m^2\end{bmatrix} \tag{32}$$

The total contribution of each mode to the detuning will be given by the superposition of each mode (33) .

$$\Delta\omega(t) = \Delta\omega_0 + \Delta\omega_0(t)' + \sum_{m=1}^{M}\Delta\omega_m \tag{33}$$

ω_m is the m-th mechanical resonance and Q_m its quality factor. The K_m coefficient can be determined using modal analysis. By sinusoidally modulating the radiation pressure on the cavity wall at frequency ω_m the steady state solution can be solved for K_m, after reconstructing $\Delta\omega_m(t)$ from an experimental measure of the cavity phase.

f_m	Q_m	K_m
53	2	0.2
89	1	0.2
191	2	0.2
278	5	0.2
439	2	0.2

Table 3: First five mechanical modes for an European XFEL cavity

The above values are obtained from a fit of experimental data and they can vary across different cavities.

To compensate the dynamic Lorentz detuning using a feedforward scheme, a reference signal of the detuning is needed. Even though the above model is used in simulations, the signal to use during compensation can be also collected experimentally, avoiding the use of a cavity model.
Using the same RF detector of the LLRF control system it is possible

to collect the cavity detuning during operation from the phase shift of the accelerating voltage using relationship (21). Microphonic contribution to the detuning can be reduced by averaging across multiple pulses.

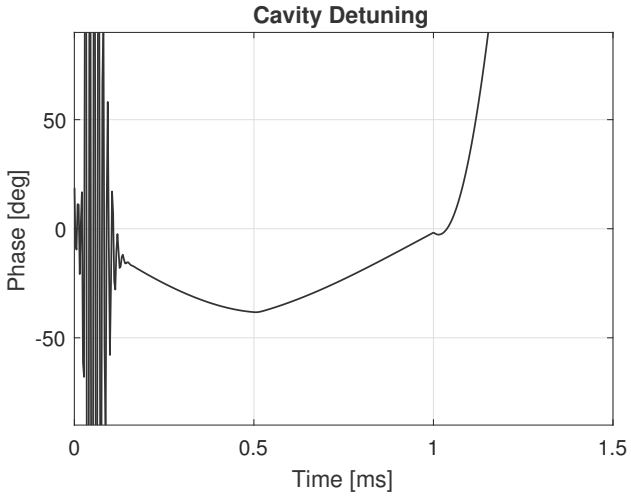

Figure 10: Simulated phase shift from a TESLA cavity operating in the XFEL.

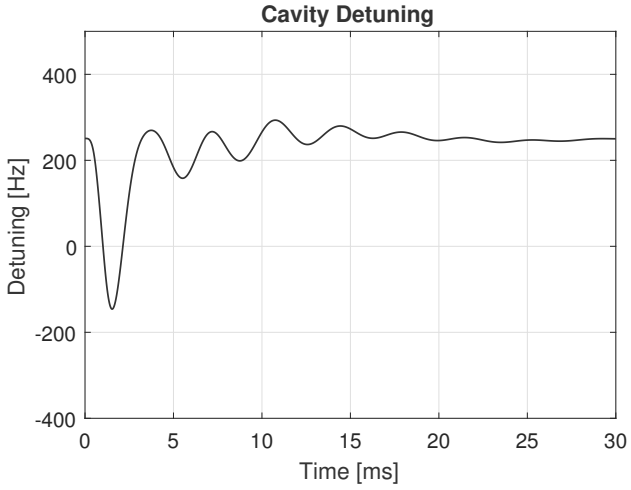

Figure 11: Simulated cavity detuning during pulsed operation of the TESLA cavity for the XFEL.

In figure (10) and (11) the phase shift and detuning of an European XFEL TESLA cavity during pulsed operation are presented. The pulse lasts 1.3ms, with a flat-top stage of 800µs. As relationship (21) was derivate in steady-state it does not hold outside the flat-top stage of the pulse and it is not possible to reconstruct the detuning from the measurable phase-shift using it. More general solutions that takes into account the dynamic behaviour of the detuning in the RLC model (making it a nonlinear system) are available and have been successfully implemented in FPGAs allowing real-time detuning compu-

tation [21]. For the purpose of the mechanical compensation during the flat-top stage the inaccessibility of the detuning in fill stage will be show not to be a limiting factor. In (11) a longer time scale is simulated to show the damping of the mechanical resonances excited by the Lorenz forces during the pulse.

3

MECHANICAL TUNERS

In the previous chapter it has been shown how Lorentz forces acting on the cavity walls and external vibrations are the main cause of detuning, the shift of the resonating frequencies of the cavity from the desired value with a consequent loss of efficiency and beam quality. In the presence of detuning the LLRF control system is able to maintain the desired accelerating voltage by increasing the injected RF power. Mechanical compensation of cavity deformations allows to maintain the resonant frequency at the desired value avoiding the increases of injected power by the LLRF control system. With this goal different designs of *mechanical tuners*, devices capable of regulating the resonant frequency of a cavity even during operation, have been proposed and employed in LINACs. In this chapter it will be given a quick overview of some common designs, including the one in use at the European XFEL, giving particular attention to the dynamic compensation of detuning during operation using piezoelectric actuators. The mechanical coupling of the tuner with the cavity is in fact not trivial and experimental models of the tuner-cavity system have highlighted the presence of numerous resonances and anti-resonances in the frequency range of interest. The characteristics of the tuner will justify the choice of the control approach applied to the resulting tuner-cavity system.

3.1 TUNERS

In chapter 2 it was shown how variations in the cavity volumes during operation cause a detuning of the resonant mode of the cavity (28). This suggests that it is possible to control the frequency of the accelerating resonant mode by causing an overall internal volume change in the cavity via a deformation of its walls. In practice this volume change is accomplished by regulating the cavity length using mechanical devices driven by stepping motors and piezoelectric tuners. The main differentiating factor among the common designs consists in the mechanical coupling to the cavity. The Blade design is an example of a coaxial mechanical tuner for TESLA cavities where the movement of the stepping motor is translated along the symmetry axis causing a deformation of the cavity in length [4]. In the European XFEL a Saclay tuner based design was chosen, where the cavity length is modified via a lateral-pick-up mechanism [15]. The stepping motor acts on a spindle connected to a lever system that exercise pressure on the cavity from one end resulting in an increase of its length. The mechanical

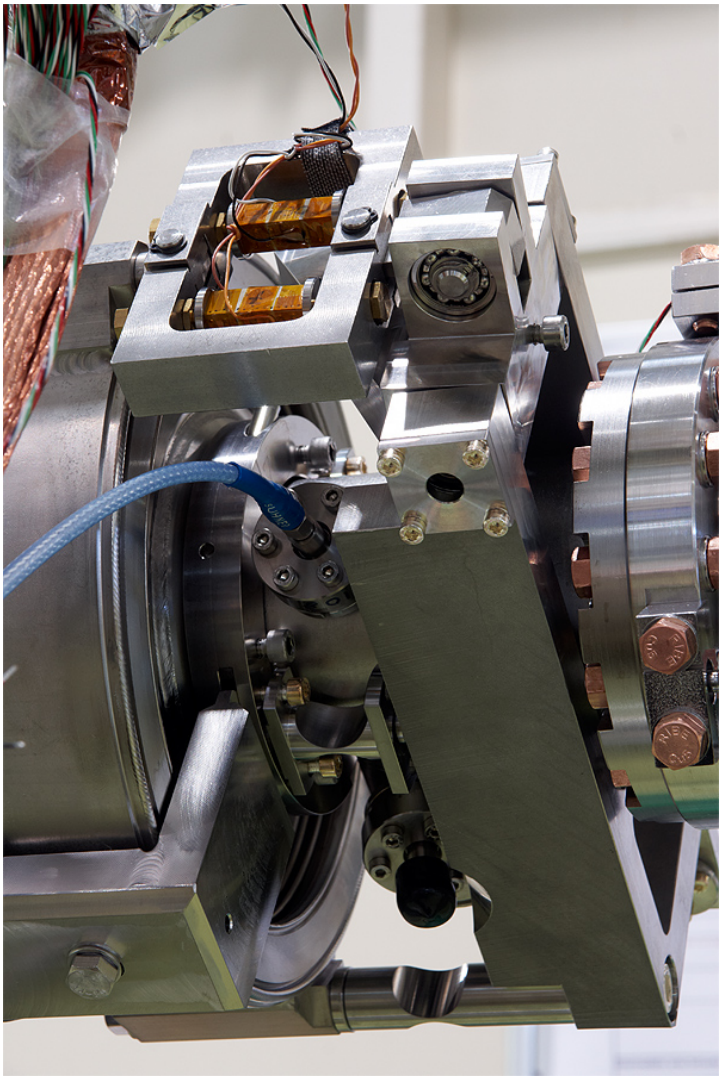

Figure 12: Saclay I Tuner

The modified Saclay I tuner in use at the European XFEL. The piezoelectric actuators, providing dynamic detuning compensation, are highlighted in orange.

system is attached to the cavity with fixtures applied to the same end before the first cell, as shown in figure (12). On one of the attachment, in place of a simple rod, the piezoelectric actuators are located to provide the speed and resolution not allowed by the stepping motor. Both the Blade and the Saclay designs are entirely contained in the cryogenic vessel (cryostat) and their dimensions along the plane perpendicular to the cavity axis are comparable with the dimensions of the cavity itself. The Slide-Jack tuner is instead an example of tuner design with both coaxial and lateral action on the cavity whose driver is collocated outside the cryostat. This design allows, in addition to the stepping motor, a full manual regulation of the cavity length.

	Blade	SaclayI	Slide − Jack
Type	Coaxial	Lateral-Pick-up side	Coaxial and Lateral
Drive Unit	Inside	Inside	Outside
Frequency	1.3GHz	1.3GHz	1.3GHz
Tunable Range	600kHz	500kHz	900kHz
Sensitivity	1.5Hz/step	1Hz/step	3Hz/step
Piezo	2,thin-layer (0.1mm)	2,thin-layer (0.1mm)	1,thick-layer (2mm)
Piezo Voltage	200V	200V	1000V
Piezo Stroke	55µm	55µm	40µm
Piezo Cap.	8µF	8µF	0.9µF

Table 4: Figures of merit for different mechanical tuners [25].

It should be noted that the sensitivity of the above tuning systems does not translate in practice to such an accuracy on the cavity tuning. Typically a millimeter change in cavity length causes a detuning of 315kHz [2]. Having a sensitivity in the order of 1Hz/step for the coarse tuner means achieving step size of approximately 3 nm in a cavity of 1 m. While this sensitivity is actually achieved in practice, the hysteresis exhibited by the cavity must also be taken into account during the tuning process even in a relative restricted range (300Hz) compared to the full tunable range afforded by the stepping motor ($500 - 900$kHz). Characterization of the hysteresis of the Saclay tuner from -150Hz to 150 has shown a residual detuning of 30Hz[17], while a characterization from -2500Hz to 2500[4] has shown a value of ≈ 300Hz. In both cases a backslash effect, where movement of the stepper motor does not lead to a change in resonant frequency, was observed. All the presented tuners include, in addition to the stepping motor for coarse tuning, the piezoelectric actuator allowing fine tuning of the cavity during operation.

3.2 PIEZOELECTRIC ACTUATOR

While the coarse tuners are capable of tuning the cavity over an extended range of frequencies their low resolution and speed make them inadequate to the compensation of dynamic detuning, where due to Lorentz forces large variations of the resonant frequency (up to 600Hz) occur in a $1-2ms$ time window. In all the previous designs piezoelectric actuators are mounted along the symmetry axis of the cavity in a frame part of the tuning system, to provide the fast tuning ability to compensate the effects of Lorentz forces during pulsed operation.
Piezoelectric actuators are a class of devices that employ the piezoelectric effect commonly used to either measure vibration, deformations or displacements, (direct piezoelectric effect), or to compensate them (inverse piezoelectric effect). Many kind of materials showing piezoelectricity are used in the construction of piezoelectric actuators or sensor [24]. Quarz, lithium niobate and lithium tantalate are the most common crystals employed in single-crystal devices, including frequency stabilized oscillators, extensively used as clock sources, and surface acoustic devices. Thanks to the ability to change their piezoelectric properties, polycrystalline materials are the most used and studied for actuators and sensors. In particular ceramics made of solid solutions of lead zirconate titanate (PZT), $(Pb(Ti,Zr)O_3)$, have shown piezoelectric properties that have led to their use in high performance actuators and are the one employed in linear accelerators for the compensation of detuning [4].
For the Blade and Saclay tuner designs stack actuators are used. These are multilayer actuators in which many (100-500) thin (aproximately $100\mu m$) layers of piezoelectric/electrorestrictive ceramic material are stacked on top of each other. The main advantages in respect to the bimorph designs, where instead piezoelectric and elastic plates are bonded together, are a faster response delay, ($10\mu s$) compared to ($1ms$), and higher generative force, in the order of kN compared to N. The latter is particularly important due to the high stiffness of the tuner-cavity system. The main disadvantage is a lower displacement that limits their cavity tuning range, a requirement that must be taken into account also due to the deterioration of the piezoelectric performance at cryogenic temperature compared to room conditions.
As seen in chapter 2 Lorentz forces acting on the cavity walls can lead to a detuning of several hundred hertz, depending on the desired accelerating voltage. The piezoelectric actuator therefore should be capable to offer a sufficient displacement. A tuning range of 850Hz is considered a requirement for the compensation of Lorentz forces in XFEL cavities capable to operate at high gradients ($35MV/m$)[20]. This corresponds to a displacement of $\approx 3\mu m$ that has to be realized by the piezoelectric actuator at cryogenic temperature. Typically ac-

tuators manufacturers do not publish technical specifications at cryogenic temperatures, and different performance deterioration of different actuators lead to the necessity of conduct a new characterization in the working condition of the cavity.

	Noliac	Noliac	Epcos	PI
Material	PZT-S1	PZT-S2	PZT-nd34	PZT-PIC 255
Layers	266	490		300
Layer Thickness	140 µm	140 µm		113 µm
Max Stroke	60 µm	100 µm	40 µm	35 µm
Max Stroke (4K)	7 µm	12 µm	8 µm	7 µm
Capac.	8 µF	40 µF	2.1 µF	12.5 µF
Capac. (4K)	1 µF	4 µF		

Table 5: Figures of merit for different piezoelectric actuators [4].

In table 5 the performance deterioration of different piezoelectric actuators used in linear accelerating cavities are shown. Typically the maximum stroke is reduced by a factor of 5-10 or more and actuators that seemed fit to operate in superconductive cavities (ex. a series from JENA, stroke @ 300 K $\approx 40\mu m$, not in the table) had to be discarded after the characterization at cryogenic temperatures [10].
Along with the reduction of maximum stroke the actuator capacitance also decreases, with a linear correlation at temperatures lower than 100 K. Since each piezo in a linear accelerator (one for each cavity, nearly a thousand in the European XFEL), needs to be calibrated, measuring the capacitance was proposed as faster and simpler mean to retrieve the displacement as oppose to a more complex direct measure.
Operating these actuators at low (4 K) temperatures does not introduce only additional difficulties. Piezoelectric actuator are commonly affected by hysteresis introducing a nonlinearity in their behaviour. At liquid helium temperatures the hysteresis of the piezoelectric *itself* is negligible [10] but not the one of the overall structure of the tuner-cavity system, making the hysteresis observed during piezoelectric actuator action dependent on the tuner design with errors varying in a order of magnitude for the same displacement. A characterization of the hysteresis for the piezoelectric actuator in the Blade tuner as shown an error up to 200 Hz in a 1200 Hz range compared to the approximated linear behaviour [4]. The European XFEL, that will be considered during simulations, employs instead a Saclay tuner that

show a reduced hysteresis with a maximum error of 25 Hz in the same 1200 Hz tuning range. (13) [8].

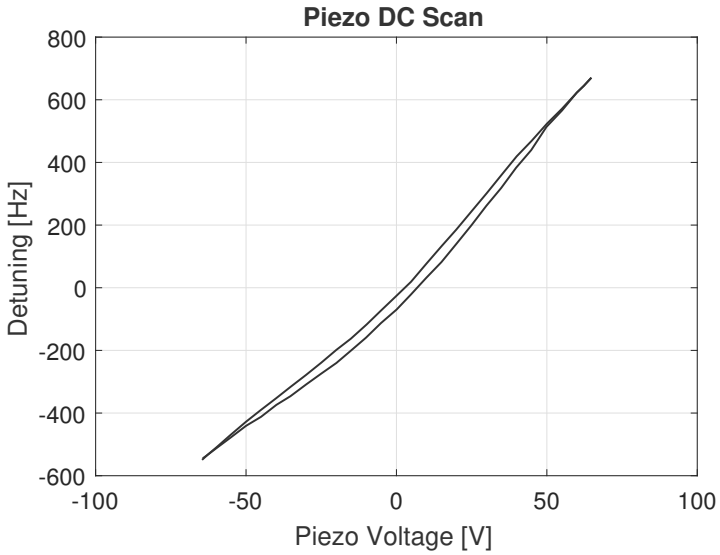

Figure 13: Hysteresis from piezoelectric action of an European XFEL tuner The graph was reconstructed from experimental data available in [8].

During the RF pulse the piezoelectric actuator is actually expected to offer compensation in a lower range resulting in a smaller hysteresis. In the European XFEL during typical operation the resonant frequency shift from Lorentz forces reach 600 Hz (accelerating gradient of 25 MV/m) but due their relative slow dynamics compared to the pulse length (1.3 ms) only a shift of 350 Hz needs to be compensated. This reduces errors induced by hysteresis sufficiently below the cavity bandwidth (250 Hz) and can thus be neglected during the feedforward pulse compensation.
In addition to have sufficient displacement to cover the detuning due to Lorentz forces in pulsed operation the piezoelectric actuator also needs to have sufficient resolution to be able to compensate microphonic detuning during CW operation. The theoretical minimum step size of the piezoelectric actuators employed is approximately 0.2nm corresponding to a detuning of 0.06Hz. In practice the presence of the hysteresis leads to a lower resolution. In [17] the piezoelectric hysteresis over a limited frequency range (1.5Hz) was characterized. Taking into account the effects of the hysteresis a real resolution of 0.2Hz was achieved, allowing operation at a very narrow (less than 5 Hz) bandwidths.

3.2.1 *Model*

To conduct simulations involving the piezo actuator a model reproducing the main features of the tuner-cavity system was reconstructed

on the basis of physical considerations of the system. The tuner is mechanically coupled to the cavity forming, for the purpose of the study of the transfer function from the piezoelectric actuator to the cavity detuning, a cavity-tuner system characterized by its own mechanical resonances. In the case of Lorenz detuning the deforming electromagnetic pressure acts on the overall structure of the cavity while the piezoelectric force is applied in a small section. In general the mechanical modes excited by the action of the piezoelectric will differ from the modes excited by the Lorentz detuning.
An estimation of the cavity-tuner system function can be obtained experimentally by sweeping the operating frequency of the drive unit operating the piezo. The cavity is operated in CW and to the drive of the piezoelectric actuator is fed a sinusoidally oscillating signal at a chosen frequency. The resonant frequency of the accelerating mode for the RF field of the cavity similarly oscillates, after a transient, at the same frequency of the drive signal as a sinusoids. The amplitude of the resulting sinusoidal oscillation is then recorded along with its phase respect to the signal driving the piezo. The procedure is then repeated for a set of frequencies obtaining the frequency response of the cavity-tuner system from the driver of the piezoelectric actuator to the detuning of the accelerating mode of the cavity [13][9].
A time-resolved approach can also be used to provide an estimate of the transfer function. In this case the piezoelectric tuner is used as a sensor (direct piezoelectric effect) during repeated pulsed operation. The resulting collected voltage signal is then used to provide an estimation of the transfer function[3]. In [5] the frequency response of the piezoelectric tuners used in the European XFEL was characterized using the latter approach. The main identifiable features are two resonances at 250Hz and at 820Hz. In figure (14) a simplified transfer

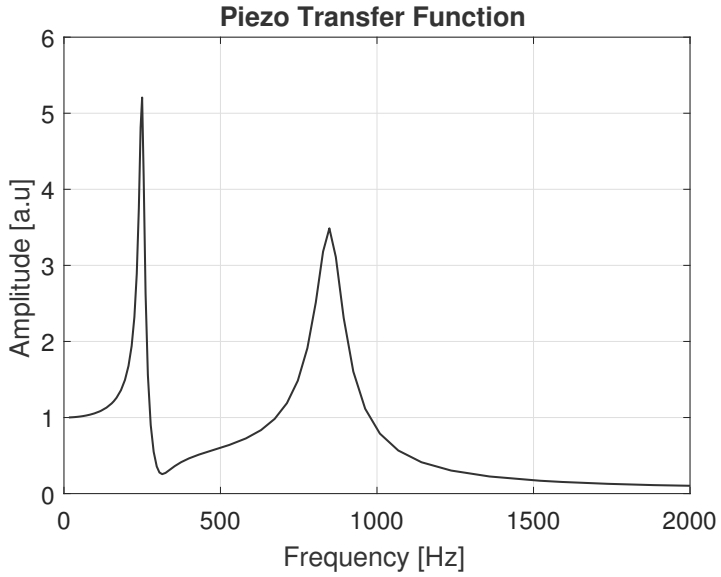

Figure 14: Dominant resonances of the cavity-tuner system.

function, that includes the two main resonances, is shown.
To construct a simplified model of the tuner-cavity system transfer function, the time estimation from [5] was considered. Apart from visible resonances shown by the signal of the piezoelectric when used as a sensor, the transfer function must also take into account the driver and time delays. The first term we consider is a low pass filter given by the piezoelectric driver:

$$H_{lp}(s) = \frac{\omega_p}{s + \omega_p} \tag{34}$$

Usually the pole is located at 500Hz well below the resonant frequencies of the piezoelectric (above 50kHz for the actuators typically used). To this term the delay given by the control delay given by the piezoelectric actuator and the group delay of the acoustic waves in the cavity must be added:

$$H_{delay}(s) = e^{-\tau \cdot s} \tag{35}$$

In practice the piezoelectric actuator exhibit a great number of smaller resonances and anti-resonances given by the mechanical coupling of the cavity-tuner system. For this simulations only the two dominant resonances were considered, parametrized with their frequencies ω_k and dumping coefficients ξ_k.

$$H_k(s) = \frac{\omega_k^2}{s^2 + 2\xi_k\omega_k + \omega_k^2} \tag{36}$$

The overall transfer function from the driver of the piezoelectric actuator to the detuning of the accelerating resonance of the cavity is therefore given by:

$$H(s) = \left(\sum_k H_k(s) + H_{lp}(s) \right) \cdot H_{delay}(s) \tag{37}$$

Such a model is not going to be a good approximation of the actual system and as such it cannot be used to synthesize a controller or feedback filter for a real cavity. It will only be used to produce simulated data on which to test the control approach proposed in the next chapter.

4

CONTROL APPROACH

In the previous chapter it has been shown how piezoelectric tuners inserted into the tuning system attached to the external walls of the cavity are able to shift the resonant frequencies for the electromagnetic field and therefore are potentially capable of compensating cavity detuning during operation.
In linear accelerators, such as the LINACs in operation in the European XFEL, piezoelectric tuners are successfully employed to compensate Lorentz detuning using iterative adaptive control schemes [21]. Since the Lorentz detuning during a pulse is known, a pulse of opposite sign is fed through a feedforward filter to the piezoelectric actuator and the resulted detuning is used to update the filter coefficients for the next pulse. In continuous wave operation feedback control schemes, and schemes involving both a feedback and feedforward paths have been show to be able to reduce the effects of microphonic noise [17].
In the following chapter will be proposed an application of non iterative direct control methods for the compensation of Lorentz and microphonic detuning, employing respectively a feedforward and feedback control path.

4.1 SYSTEM SCHEME

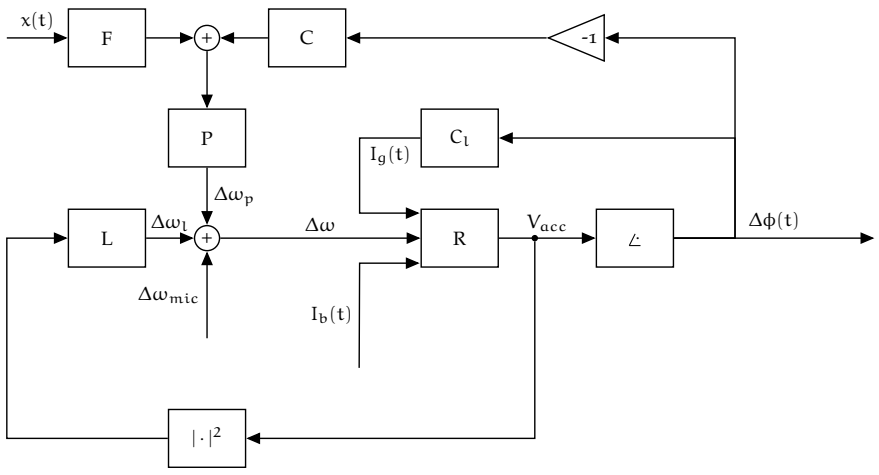

Figure 15: Cavity detuning control scheme

We've previously seen in chapter 2, while describing the effects of detuning on beam acceleration, a model for the radio frequency behaviour of the cavity and a model for the detuning caused by Lorentz

forces. While those have been considered independently to provide an explicit solution to the cavity differential equation, they are coupled together via the detuning term $\Delta\omega_l$, the Lorentz detuning, as show in scheme (15). During operation the accelerating voltage of the cavity causes a detuning due to the Lorenz forces which in turn causes a variation of the accelerating voltage. The same consideration is valid for the contributions of the piezoelectric actuator. As seen in chapter 3, P represent the transfer function of the piezoelectric actuator attached to the cavity, from the actuator voltage to the detuning of the resonant frequency of the accelerating mode. Its contribution, indicated with $\Delta\omega_p$ is superimposed to the contribution of the Lorentz forces, modeled by the model L, and to the microphonic noise $\Delta\omega_{mic}$. The radio frequency model of the cavity R, in a similar way to the simplified model shown in section 2.1, takes as inputs the detuning, the Klystron current and beam current and gives as output the accelerating voltage. By remembering the RLC equation for the accelerating voltage of the cavity (12), and the model for the Lorenz detuning (32), we can notice that the overall system is nonlinear. It therefore would appear that methods for the synthesis of both the feedfoward filter and the feedback filter for linear systems cannot be applied.

From the diagram we can see that the Low Level Radio Frequency (LLRF) control, responsible for the resonating RF field and hidden in the nonlinear block C_l, forms an inner loop containing the RF model of the cavity. The LLRF control system, which has not been treated in detail, hides the nonlinearities to the outer loop by making the amplitude of the accelerating gradient independent from $\Delta\omega$ (and I_b) while its phase remains correlated to it. This decouple the radio frequency model of the cavity R from the effects of Lorentz detuning, only dependent on the modulus of V_{acc} and not its phase. The LLRC controller is thus performing a feedback linearization for the dynamics of the cavity resonant frequency. As a consequence the closed loop containing the contribution of Lorentz detuning is cut, reducing it to a known disturbance on the output of P. Furthermore, since the relationship between the phase of the accelerating voltage and the detuning is known, the phase can be used to recover the detuning from the RF detector. Under the assumption of a correctly working LLRF control system and detector the control scheme with the hidden inner loop is reduced to (16). While the block R_c, hiding the inner loop formed by the LLRF control system, is in general non linear, under the assumption of a ideal action from the Klystron its model is known. Remembering equation (21), we can retrieve the detuning minus a multiplicative constant during flat-top operation without using any cavity parameters. This allows to restore linearity to the detuning compensation feedback loop under a condition that is not restrictive in practice neither for the synthesis of the feedback controller nor the

feedforward filter justifying the use of synthesis methods for linear systems.

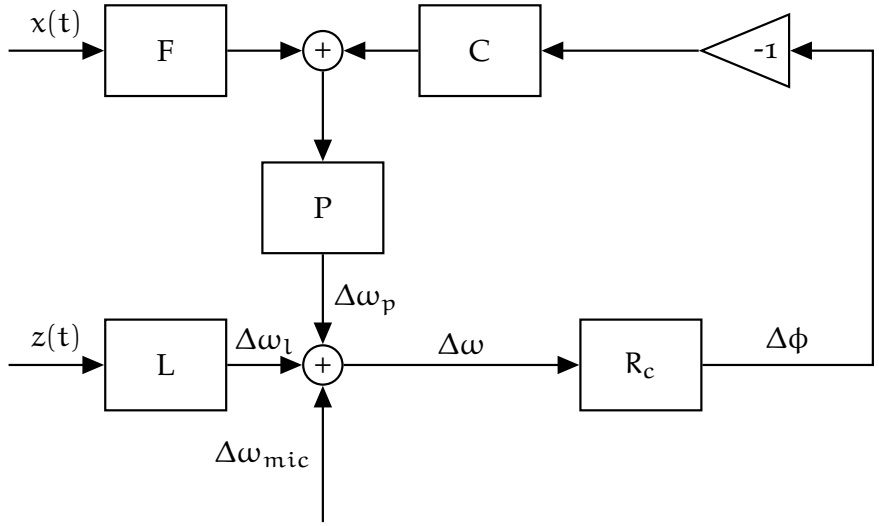

Figure 16: Simplified cavity detuning control scheme

4.2 CONTROL SCHEME

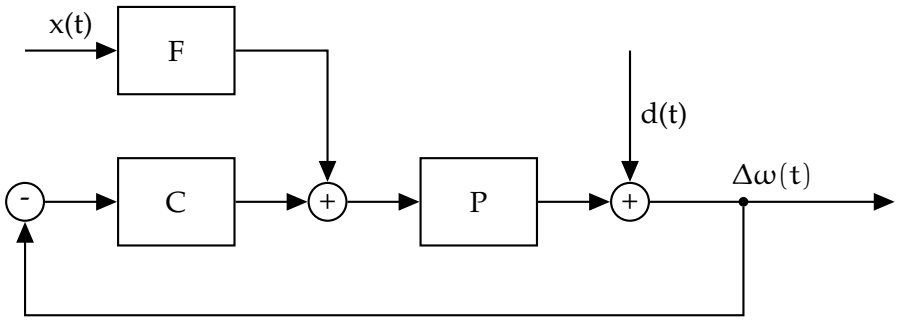

Figure 17: Detuning compensation scheme.

In figure (17) the control scheme that is going to be considered is presented. The plant P represents the tuner-cavity-tank system having the piezoelectric driver voltage as input and the detuning of the cavity as output. The cavity detuning is calculated using (21), where the phase of the accelerating voltage is measured using the RF detector, already employed in the LLRF control system. It should be noted that (21) is limited to the flat-top stage and does not hold during the fill and decay stages. This does not constitute a limit in practice. In continuous wave the cavity remains in the flat-top stage during operation and so no sampling problem is present. In the pulsed regime detuning sampling is possible only during the flat-top stage of each pulse, leading to a limit of the sampling frequency for compensation

of 10 Hz [22]. Such rate is still sufficient to compensate all or part of the low frequency microphonic background.
The disturbance $d(t)$ includes the contributions to detuning from both the Lorentz forces and the microphonics.
For the feedback controller C a simple PID is used, but the synthesis method employed, VRFT, is only limited to controllers linear in their adjustable parameters and therefore the optimal controller could be looked in a more general class. The reference signal to the feedforward filter $x(t)$ is constructed by inverting the sign of the detuning due Lorentz forces during operation in the flat-top stage, possibly averaged to reduce noise. The feedforward filter F, ideally a stable approximation of the inverse of the plant P in the frequencies excited by the reference signal, filters $x(t)$ obtaining the voltage signal for the piezoelectric actuator compensating Lorentz detuning.
As seen in chapter 3 P, the piezoelectric actuator shows a good linear behaviour justifying the use of linear control for detuning compensation.

4.3 DIRECT METHODS

The transfer function of the tuner-cavity-tank system, indicated previously with P, exhibit a complex behaviour, including numerous resonances and anti-resonances, due to the coupling of all the mechanical structures in which vibrations from the cavity can be transmitted. In the absence of theoretical models capable to predict the frequency shift of the RF resonant mode of the cavity from the piezo displacement, the piezoelectric tuner has been characterized by estimating its transfer function from input/output data. Traditional model-based control (MBC) employs these models in the synthesis of the controller according to the certainty equivalence principle: the estimated model is used in place of the real model, as it it were the true one, while looking for the desired controller. The accuracy of the estimation is therefore an important concern regarding both the performance and stability of the closed loop system. Currently model estimation has been conducted via the frequency domain analysis of the system [9][16][1]. Models obtained have shown an important number of resonances even in a limited frequency range leading to hundreds of parameters necessary to reconstruct the system dynamics (120 for a range of 10-200 Hz in [17]). This has prevented the use self-tuning methods, where an estimate of the model is update online, due to an excessive computational cost both in digital signal processor (DSP) and field programmable gate array (FPGA) implementations. The

1 The signal to the piezoelectric actuator is sinusoidally modulated and confronted with the resulting steady-state sinusoidal oscillation of the cavity resonant frequency. The resulting amplitude ratio and delay respect to the piezo driving signal is collected for a set of frequencies to reconstruct the frequency response of the tuner-cavity system.

difficulties in producing an accurate model of the system combined with its high order has led to reject the use of MBC. In contrast data driven control (DCC) methods allows the synthesis of the feedback controller or the feedforward filter from a set of input/output measurements without the intermediate step of constructing an estimate of the model.
Iterative direct methods have already been successfully employed both in the compensation of Lorentz detuning at the European XFEL [21], and in the compensation of microphonic detuning [17]. Iterative Feedback Tuning (IFT) and Iterative Learning Control (ILC) are direct methods that has been employed in a variety of application and have been show to produce results as good as, or better, than the most common non direct method for the synthesis of the feedback controller or feedforward filter in presence of uncertainties on the plant model. In these methods multiple iteration are performed to minimize the respective cost functions using an approximation of the gradient of the cost function itself constructed from experimental data at each step. However the iteration procedure has the unwanted effect to produce an overall nonlinear device that can exhibit complex behaviour. The implementation of an iterative least-square based feedforward algorithm for the compensation of microphonics has shown that convergence to a stable and effective filter depends on the initial conditions and manually tuned iteration parameters [17].
In contrast non-iterative methods, where the controller is synthesized offline, preserve the linearity of the controlled system while avoiding convergence issues during operation. To this end the Virtual Reference Feedback Tuning (VRFT) and the Correlation Approach are proposed for the synthesis of a feedback controller and a feedforward filter. Both are non-iterative direct control methods that allow an offline synthesis from sets of input/output data. Additionally when considering a class of linear controllers in their parameter vector their respective cost function admit an explicit solution in the form of the least squares formula. In this sense these method correspond to a one-shot solution to the control problem, with no experimental iterations, where only sets of input/output data are required. The main drawback compared to the iterative methods is the loss of the ability to adapt during operation to changes in the behaviour of the system, for example due to the heating of the piezo actuator [19].

4.3.1 *Direct Feedback Design*

Virtual Reference Feedback Tuning (VRFT) is a direct non-iterative method for the synthesis of a feedback controller from a pair of input/output measurement. In the following section will be given an introduction of its offline variant as employed for the detuning compensation scheme for the TESLA cavity as described in [7].

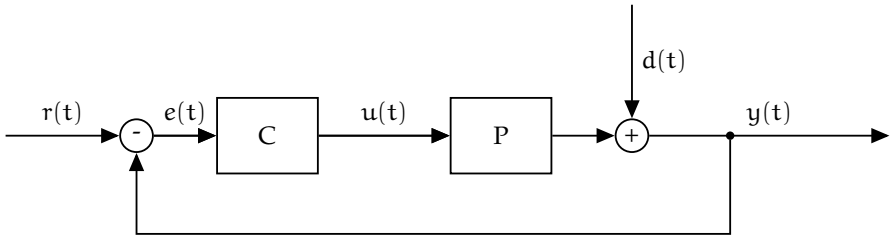

Figure 18: Feedback control scheme with disturbance.

Considering a closed loop system where P is an unknown linear plant and C is feedback controller, we are interested in choosing C to obtain the desired behaviour for the controlled system. C will be chosen between the class of controllers with parameter vector θ:

$$\theta = \begin{bmatrix} \vartheta_1 & \vartheta_2 & \dots & \vartheta_n \end{bmatrix}^T \tag{38}$$

The closed loop behaviour of the controlled system is given by:

$$M(z;\theta) = \frac{C(z;\theta)P(z)}{1 + C(z;\theta)P(z)} \tag{39}$$

Ideally we would like to find a vector of parameters θ so that the closed transfer function M will be equal to a M_0, the transfer function of the system with the desired behaviour. In general such vector does not exists, so instead we try to minimize a distance between the behaviour of the system controlled by $C(z;\theta)$ and M_0. A *model-reference* cost function can be defined:

$$J_{MR}(\theta) = \left\| \left(\frac{P(z)C(z;\theta)}{1 + P(z)C(z;\theta)} - M_0(z) \right) W(z) \right\|_{L^2}^2 \tag{40}$$

$$J_{MR}(\theta) = \frac{1}{2\pi} \int_{-\pi}^{\pi} \left| \frac{P(e^{j\omega})C(e^{j\omega};\theta)}{1 + P(e^{j\omega})C(e^{j\omega};\theta)} - M_0(e^{j\omega}) \right|^2 \left| W(e^{j\omega}) \right|^2 d\omega \tag{41}$$

W is a weighting term that can be use to give more importance to the behaviour in a chosen frequency range.
As J_{MR} depends on the unknown plant P it cannot be minimized. VRFT sidestep the problem be introducing a new cost function, the *virtual reference* cost function J_{VR}, in which the plant P does not appear explicitly and whose minimum approximate the minimum of J_{MR}.
To introduce J_{VR} we can consider the following scheme:

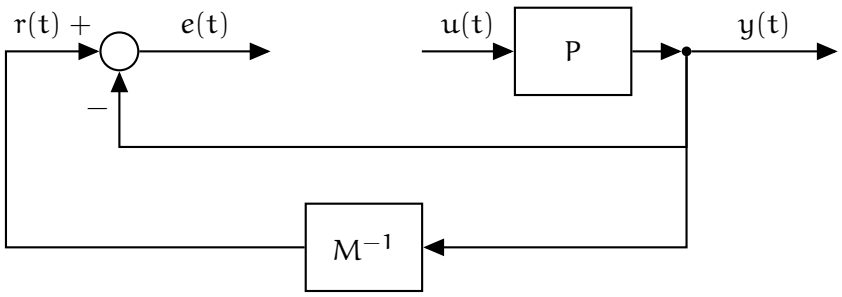

Figure 19: Scheme for the synthesis of the feedback controller.

On the unknown plant P we can conduct an input/output experiments, obtaining an output $y(t)$ from an input $u(t)$.
For the closed loop system (20) it exists an input $r(t)$ such that the output $M(z)r(t)$ will be equal to $y(t)$, or in others words, it exists an input for the closed loop system such as to give the same output of the plant when driven by $u(t)$. Such input can be immediately obtained $\bar{r}(t) = M^{-1}(z)y(t)$. Since all the calculations are offline $M^{-1}(z)$ does not need to be proper and so $\bar{r}(t)$ can always be calculated.
Considering the closed loop system we can introduced the virtual error $\bar{e}(t) = \bar{r}(t) - y(t)$. For C to be a good controller for P when fed the virtual error it should output $u(t)$, the input signal that fed to the plant outputs $y(t)$.
Therefore it is a necessary condition for the ideal $C(z;\theta_0)$ to have $u(t) = C(z;\theta_0)e_v(t)$. In general we cannot expect to find such a controller but we can ask to have C as closed as possible to it, meaning its output should be as close as possible to u(t):

$$J_{VR} = \frac{1}{N}\sum_{t=1}^{N}(u(t) - C(z;\theta)e_v(t))^2 \tag{42}$$

The new cost function introduced is not equivalent to J_{MR}, and so needs to be modified to recover an equivalent, or more generally an approximately equivalent, cost function to J_{MR}. In (40) we could give different weights to different frequencies using W. To recover this ability the filter $L(z)$ can be introduced to J_{VR}.

$$u_l(t) = L(z)u(t); e_l(t) = L(z)e_v(t) \tag{43}$$

$$J_{VR} = \frac{1}{N}\sum_{t=1}^{N}(u_l(t) - C(z;\theta)e_l(t))^2 \tag{44}$$

In general finding the absolute minimum of the J_{VR} means minimizing a nonlinear scalar function over the vector variable θ which is not a trivial task. Instead we consider a class of linear controllers in their parameter vector θ. Such controllers can be written using as a basis a vector of linear transfer functions $\beta(z)$:

$$\beta(z) = \begin{bmatrix}\beta(z)_1 & \beta(z)_2 & \dots & \beta(z)_n\end{bmatrix}^T \tag{45}$$

And the resulting controller is given by:

$$C(z;\theta) = \beta(z)\theta \tag{46}$$

The VRFT cost function is now a quadratic function, admitting a single minimum, that can be explicitly solved by the least squares formula:

$$\hat{\theta}_N = \left[\sum_t^N \varphi_l(t)\varphi_l(t)^T\right]^{-1}\left[\sum_t^N \varphi_l(t)u_l(t)\right] \tag{47}$$

where:

$$C(z;\theta)e_l(t) = \beta^T(z)e_l(t)\theta = \phi_l^T(t)\theta \tag{48}$$

In general the virtual reference cost function J_{VR} differs from the model reference cost function J_{MR}, and so the minimizing parameter vector will also be different. By an appropriate choice of $L(z)$ it is possible to minimize the distance between the two minima.

$$L^*(z) = \frac{W(z)M(z)(1-M(z))}{G(z)} \tag{49}$$

$$G(z) = \left|G(e^{j\omega})\right|^2 = \Phi_u \tag{50}$$

Where $\Phi(u)$ is the spectral density of $u(t)$. Since $u(t)$ is chosen for the input/output experiment the pre-filter $L^*(z)$ can be computed. We can justify (49) by substituting it in J_{VR} and comparing the obtained cost function with J_{MR}.

$$\begin{aligned} J_{MR}(\theta) &= \frac{1}{2\pi}\int_{-\pi}^{+\pi} \frac{|P|^2\,|C_0 - C(\theta)|^2}{|1+PC_0|^2\,|1+PC(\theta)|^2}\,|W|^2\,d\omega \\ J_{VR}(\theta) &= \frac{1}{2\pi}\int_{-\pi}^{+\pi} \frac{|P|^2\,|C_0 - C(\theta)|^2}{|1+PC_0|^2\,|1+PC_0|^2}\,|W|^2\,d\omega \end{aligned} \tag{51}$$

The only approximation of the virtual reference cost function is a substitution of a $C(\theta)$ at the denominator with the ideal controller C_0. J_{VR} is not, across all possible values for the parameter vector θ, a good approximation of J_{MR} since $C(\theta)$ can differ much from C_0. But *it is* a good approximation in its minimum, which is the only point we are interest in and that can immediately solved using the least squares formula (47). The minimum for J_{MR} is, if the controller class is reasonable chosen, a controller approximating C_0, and J_{VR} is justified as good approximation of J_{MR} in its minimum.
Until now the case of an input/output experiment has been considered in absence of noise on the system output. In an experimental setting the output of the plant will be affected by a non white noise $d(t)$.

The virtual reference cost function remains (44) but the virtual error $e_l(t)$ includes now the effect of the disturbance on the output. To

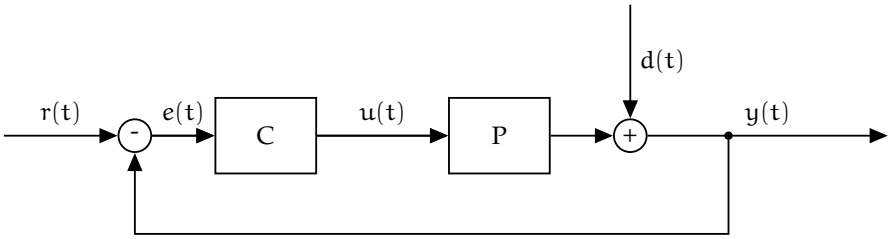

Figure 20: Feedback control scheme with disturbance.

study the effects of $d(t)$ we can consider the asymptotic case, obtaining for J_{VR} the following expression in the frequency domain:

$$\begin{aligned} J_{VR}(\theta) = \frac{1}{2\pi}\int_{-\pi}^{+\pi} \frac{|P|^2\,|C_0 - C(\theta)|^2}{|1+PC_0|^2\,|1+PC_0)|^2}\,|W|^2\,d\omega + \\ + \frac{1}{2\pi}\int_{-\pi}^{+\pi} \frac{|C(\theta)|^2}{|C_0|^2}\frac{|L|^2}{|P|^2}\Phi_d(\omega)d\omega \end{aligned} \tag{52}$$

The virtual reference cost function in presence of noise is not consistent: the noise influences the position of the minimum with the term on the second line regardless of the duration of the experiment.
L cannot be used to transform in a constant contribution the second term for two main reasons:

- We could not use L to make J_{VR} a good approximation of J_{MR}.
- We would need to known $|P|^2$ and Φ_d, both unknown.

The problem can be overcome by relaxing the requirement of a single experiment allowing the introduction of an instrumental variable (IV). Previously the explicit solution for the minimizing parameter vector $\hat{\theta}_{VR}$ was given by the least squares formula (47).
As defined, $\hat{\theta}_{VR}$ can be interpreted as an estimator for θ_0 the optimal parameter vector of the controller C. The approach consists in introducing a new estimator $\hat{\theta}^{IV}_{VR}$ that remains consistent even in the presence of the disturbance $d(t)$:

$$\hat{\theta}^{IV}_{VR} = \left[\sum_t^N \xi(t)\varphi^T(t)\right]^{-1}\left[\sum_t^N \xi(t)u_l(t)\right] \tag{53}$$

The effects of $d(t)$ in the estimator are contained in u_l, according to the control scheme:

$$u_l(t) = \theta_0^T\phi(t) + z(t) \tag{54}$$

$$z(t) = -\frac{L(z)}{P(z)}d(t) \tag{55}$$

The introduced instrumental variable $\xi(t)$ needs to fulfill two properties. First it needs to correlated with ϕ_l, so that the term $E[\sum \xi(t)\varphi_l^T(t)]$

is non singular and (53) has meaning. And secondly it needs to guarantee the consistency of the estimator, from which $\xi(t)$ needs to be uncorrelated with the disturbance $d(t)$. With those two properties $\hat{\theta}^{IV}_{VR}$ is a good estimator for θ_0. To show it we explicit the dependence of $u_l(t)$ from $z(t)$ as in equation (54):

$$\begin{aligned}
\hat{\theta}^{IV}_{VR} &= \left[\sum_t^N \xi(t)\varphi_l(i)^T\right]^{-1}\left[\sum_t^N \xi(t)u_l(t)\right] = \\
&= \cancel{\left[\sum_t^N \xi(t)\varphi_l(t)^T\right]^{-1}}\cancel{\sum_t^N \xi(t)\varphi_l(t)^T}\,\theta_0 + \\
&+ \left[\frac{1}{N}\sum_t^N \xi(t)\varphi_l(t)^T\right]^{-1}\frac{1}{N}\sum_t^N \xi(t)z(t) \\
\hat{\theta}^{IV}_{VR} &\xrightarrow[N\to\infty]{} \theta_0 + E\left[\xi(t)\varphi_l(t)\right]^{-1} E\left[\xi(t)z(t)\right] = \theta_0
\end{aligned} \tag{56}$$

Performing a second experiment allows the construction of the instrumental variable while maintaining the direct characteristic of the VRFT method.
The repeated experiment is performed using the same $u(t)$ input to the plant, but obtaining a different output, $\tilde{y}(t)$, affected by a new disturbance $\tilde{d}(t)$. $\tilde{y}(t)$is still correlated to the output of the previous experiment, ($u(t)$ is unchanged), but uncorrelated with $d(t)$, due to the general decrease of correlation in time in stochastic processes. The assumption of non correlation between $d(t)$ and $d(t+\tau)$ is verified in practice as long as a sufficient time is waited between the experiments. By constructing the instrumental variable $\xi(t)$ as:

$$\begin{aligned}
\xi(t) = \tilde{\varphi}_l(t) &= \beta(z)e_l(t) = \\
&= \beta(z)L(z)M(z)(1-M(z))\tilde{y}(t)
\end{aligned} \tag{57}$$

it satisfied the previously listed properties and $\hat{\theta}^{IV}_{VR}$ is a consistent estimator, asymptotically unaffected by noise.
The VRFT method as presented, with the use of the instrumental variable constructed from the second experiment, is applied in this thesis to the synthesis of the feedback controller for the compensation of microphonic detuning. A pseudocode description of the algorithm implemented in shown in (1).

Algorithm 1 VRFT For a Linear Controller

Experimental Data: $u(t)$, $y_1(t)$, $y_2(t)$
Parameters: Linear Filter Class $\beta(z)$, $S(z)$, $W(z)$
Output: Parameter Vector θ

procedure SIM(T, x(t))
    Return the output of the system T to the input $x(t)$
end procedure
$L(z) = (1 - M(z))M(z)W(z)/\Phi_u(t)$ ▷ Prefilter
$u_l(t) = SIM(L(z), u_l(t))$
$e_1(t) = SIM(L(z)(M^{-1}(z) - 1), y_1(t))$
$e_2(t) = SIM(L(z)(M^{-1}(z) - 1), y_2(t))$
$\phi(t) = SIM(b(z), e_1(t))$
$\xi(t) = SIM(b(z), e_2(t))$
$\theta = (\xi(t) \cdot \phi(t)^T)^{-1} (\psi(t) \cdot u_l(t))$

4.3.2 *Direct Feedfoward Design*

The correlation approach is a general approach to the direct synthesis of a feedforward, or feedback, filter. In [12] has been applied to non-iterative synthesis of a feedforward filter using just a single input/output experiment on a closed loop system. In the following section will be given an introduction in the form it was be applied to construction of the filter for the compensation scheme (17), proposed in this thesis for the detuning compensation of a TESLA cavity.
Considering a closed loop system (17) where P is an unknown linear plant and C is the feedback controller, synthesized for example by employing the VRFT method, we are interest in choosing F to obtain a good tracking of the reference signal $x(t)$, when this is not possible to accomplish with the use of the feedback filter alone. Ideally, in order to have good tracking, we would like to have the expectation value of tracking error equal to zero. Following the control scheme we can obtain an explicit expression for the tracking error:

$$e(t) = S(z)x(t) - F(z;\theta)P(z)S(z)x(t) - S(z)d(t) \tag{58}$$

Since $E[x(t)] \neq 0$ in general, but $E[d(t)] = 0$ by assumption, requiring the expectation value of the tracking error to be zero is equivalent to ask F to be the exact inverse of the plant P. If this is the case, the first two terms of (58) cancels each other.

$$e(t) = S(z)d(t) \tag{59}$$

Since $E[d(t)] = 0$ the expectation value of the tracking error is zero. We can observe that if we have good tracking, ($F = P^{-1}$), (59) is uncorrelated with $x(t)$, otherwise holds (58) and $e(t)$ is correlated with $x(t)$. Therefore asking for the filter minimizing the expectation value of the tracking error $e(t)$ is equivalent to ask for the filter making

uncorrelated $e(t)$ and $x(t)$. This change of perspective constitutes the key concept of the correlation approach.
Since in general the vector θ_0 giving a decorrelating filter F does not exists, a cost function to minimize, representing the degree of correlation between $e(t)$ and $x(t)$, is introduced. First we define an instrumental variable (IV), correlated with the tracking error $e(t)$ but uncorrelated with $d(t)$.

$$\begin{aligned} \xi(t) &= \beta^T(z)x(t) \\ \xi(t) &= \begin{bmatrix} \beta_1(z)x(t) \\ \beta_2(z)x(t) \\ \dots \\ \beta_n(z)x(t) \end{bmatrix} \end{aligned} \tag{60}$$

The correlation is given by:

$$f(\theta) = E\left[e(t;\theta)\xi(t)\right] \tag{61}$$

We define a quadratic cost function to minimize:

$$J_c(\theta) = \|f(\theta)\|_2^2 = f^T(\theta)f(\theta) \tag{62}$$

Since in practice we are limited by a finite experiment, an estimator for the correlation is needed:

$$\hat{f}(\theta) = \frac{1}{N}\sum_t^N e(t;\theta)\xi(t) \tag{63}$$

As written the cost function J_c is impossible to minimize because includes explicitly in the tracking error (58) the unknown plant transfer function P.
The issue can be overcome by constructing an estimator for $e(t)$ that depends only on measurable quantities and the filter F. The scheme in figure (21) allows an experiment from which to obtain such estimator.

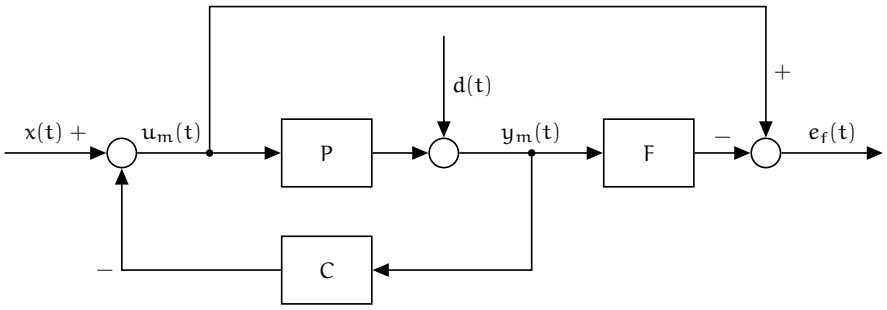

Figure 21: Scheme for the synthesis of the feedforward filter.

The system is operated in a closed loop configuration with zero as reference signal.

$x(t)$ is used as an experimental input acting as disturbance on the control signal to the plant. More generally any signal could be used, the advantages and drawbacks of a particular choice will be shown later in the frequency domain.
The experimental outputs are $u_m(t)$ and $y_m(t)$, the total control signal to the plant and its output affected by noise. By looking at the diagrams we obtain the following expressions:

$$\begin{aligned} u_m &= S(z)x(t) - SCd(t) \\ y_m &= Sd(t) + PSx(t) \end{aligned} \tag{64}$$

While looking for an estimator for $e(t)$ we can substitute the previous expressions in (58):

$$e(t) = u_m(t) - Fy_m(t) + SCd(t) - FSd(t) - Sd(t) \tag{65}$$

The explicit dependence on P has been removed, and it is now contained implicitly in the measurable signals $u_m(t)$ and $y_m(t)$. Since $E[d(t)] = 0$, the $d(t)$ terms can be removed obtaining a consistent estimator for $e(t)$.

$$\hat{e}(t) = u_m(t) - Fy_m(t) \tag{66}$$

The resulting estimator for the correlation is:

$$\hat{f}(\theta) = \frac{1}{N}\sum_{t}^{N} \xi(t)\left[u_m(t) - F(z;\theta)y_m(t)\right] \tag{67}$$

The estimator obtained is in general not linear in θ and the minimization of the cost function is a non trivial tasks involing finding the absolute minimum of a nonlinear scalar function over the variable vector θ. By chosing $F(z;\theta)$ as a linear controller in θ the estimator becomes linear and the resulting cost function can be immediatly solved for its only minimum using the least square formula. Such controller can be writtern using a vector of linear transfer function as a basis:

$$F(z;\theta) = \beta(z)\theta \tag{68}$$

$$\theta = \begin{bmatrix} \vartheta_1 & \vartheta_2 & \dots & \vartheta_n \end{bmatrix}^T \tag{69}$$

$$\beta(z) = \begin{bmatrix} \beta(z)_1 & \beta(z)_2 & \dots & \beta(z)_n \end{bmatrix} \tag{70}$$

We can explicit $F(z;\theta)$ in (**??**):

$$\hat{e}(t) = u_m(t) - \beta^T(z)y_m(t)\theta \tag{71}$$

Calling $\varphi(t) = \beta^T(z)y_m(t)$ we obtain a new expression for the correlation function.

$$\hat{f}(\theta) = \frac{1}{N}\sum_{t}^{N} \xi(t)[u_m - \varphi^T(t)\theta] \tag{72}$$

The new cost function $\hat{J}_c$, where $\hat{f}(\theta)$ was substituted to $f(\theta)$, can be immediately be solved using the least squares formula. Introducing the matrix Q and vector Z:

$$\begin{aligned} Q &= \frac{1}{N}\sum_{t}^{N} \xi(t)\varphi^{\intercal}(t) \\ Z &= \frac{1}{N}\sum_{t}^{N} \xi(t)u_m(t) \end{aligned} \tag{73}$$

Explicit solution for the estimate of the optimal parameter vector θ_0:

$$\hat{\theta}_0 = (Q^{\intercal}Q)^{-1}Q^{\intercal}Z \tag{74}$$

Previously was used the signal $x(t)$ as the experimental input for the synthesis of the filter in the tuning scheme. This choice can be justified by looking in the domain frequency at the tracking error $e(t)$.

$$J(\theta) = \frac{1}{2\pi}\int_{-\pi}^{+\pi} |\Phi_{e_x}(\omega)|^2 \, d\omega \tag{75}$$

By remembering (58) we immediately obtain:

$$J(\theta) = \frac{1}{2\pi}\int_{-\pi}^{+\pi} |S|^2 \, |1 - FP|^2 \, \Phi_x^2(\omega) d\omega \tag{76}$$

The experimental input in the synthesis experiment acts as weighting term in the frequency domain. Choosing $x(t)$ itself, the reference signal that will be fed to the feedforward filter , allows to give more importance to the range of frequencies actually used during operation. When $x(t)$ is not known in advance the synthesis experiment can still be performed by constructing an input signal with spectral power in the regions of interests.
In this thesis the correlation approach has been employed to synthetize the feedforward filter. A pseudocode description of the resulting algorithm is given in (2).

Algorithm 2 Correlation Approach for a Linear Causal Filter

Experimental Data: $x(t)$, $u_m(t)$, $y_m(t)$
Parameters: Linear Filter Class $\beta(z)$
Output: Parameter Vector θ

1: **procedure** SIM(T, x(t))
2: Return the output of the system T to the input $x(t)$
3: **end procedure**
4: $\xi(t)$ = SIM($\beta(z)$, $y_d(t)$)$^{\intercal}$
5: $\phi(t)$ = SIM($\beta(z)$, $y_m(t)$)$^{\intercal}$
6: $\boldsymbol{Q} = \xi(t) \cdot \phi^{\intercal}(t)$
7: $z = \xi(t) \cdot u_m(t)$
8: $\theta = (\boldsymbol{Q}^{\intercal} \cdot \boldsymbol{Q})^{-1}(\boldsymbol{Q}^{\intercal} \cdot z)$

4.4 SYNTHESIS PROCEDURE

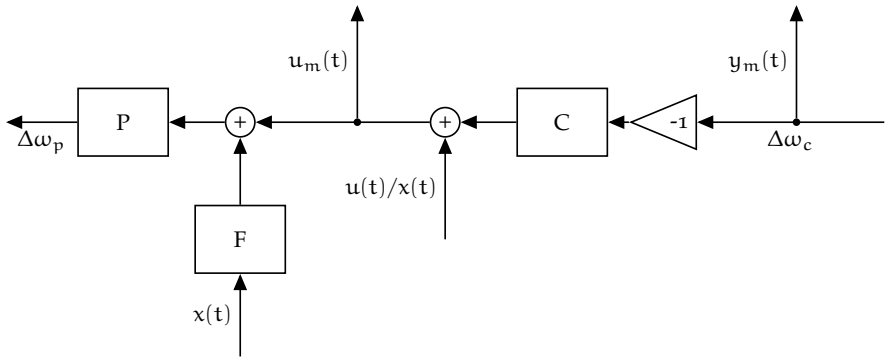

Figure 22: Piezo control with synthesis' signals.

By adding to the control scheme the signals introduced during the synthesis of both the feedback controller and feedforward signal we obtain the scheme (22). Since the correlation approach needs a closed loop experiment, the first step in the control synthesis consists in the application of the VRFT method to the synthesis of the feedback controller. The two input/output experiments, one used to construct the instrumental variable, are conducted in open loop by setting both F and C to zero. $u(t)$ correspond to the experimental input, a voltage on the piezoelectric driver, while $y_m(t)$ correspond to the experimental output, the cavity detuning. The Lorentz detuning on $y_m(t)$ is a known background, subtracted from the measured signal prior to its use in the VRFT algorithm. The third experiment for the synthesis of the feedforward filter is conducted in closed loop, using C as previously synthesized. The input signal $x(t)$ is a disturbance on the control action of the feedback controller, a voltage on the piezoelectric driver, while the two outputs are $u_m(t)$, the total signal send to the driver, and $y_m(t)$ the cavity detuning. Again the contribution of the Lorentz detuning on both outputs is a subtracted background contribution.

The necessity to subtract the experimental background given by the Lorentz forces and the cavity pre-detuning in the synthesis of both the feedback controller and feedforward filter bring the overall number of input/output experiments to five. Two for the VRFT algorithm with the instrumental variable, one for the correlation approach and the two additional to gather the background with and without feedback action. The overall parameters that influence the control synthesis are show in (6), in the next chapter a particular choice will be justified and tested on a simulated system.

Feedback Controller	
Parameter	Description
$u(t)$	Experimental Input
$S(z)$	Desired Sensitivity
$W(z)$	Frequency Weights
$\beta(z)$	Filter Class
Feedback Filter	
Parameter	Description
$x(t)$	Reference Signal
$\beta(z)$	Filter Class

Table 6: Control Parameters

5

SIMULATIONS

In the previous chapter was proposed a control scheme for the compensation of Lorentz and microphonic detuning composed by a feedforward and a feedback path. VRFT was presented has a direct method for the synthesis of the feedback controller, while for the feedforward filter was shown a correlation approach. Both synthesis methods employs only input/output experiments without prior knowledge of the model, resulting in a direct offline non-iterative approach to the control problem.
In the following chapter they will be applied to a TESLA cavity simulator set to operate at the same parameters of the cavities used in the LINACs of the European XFEL. It will be shown the feasibility of both method for the compensation of Lorentz detuning in pulsed operation and a partial compensation of microphonic detuning during continuous wave operation. A reduction of the injected power by the klystron in the accelerating cavity is shown and compared to the uncompensated case. Microphonics noise during synthesis will also be shown to not constitue a limiting factor even for relative short (in the order of senconds) experiments durations, confirming the consistency of both methods for the synthesis of the feedback controller and feedforward filter.

5.1 TESLA MODEL

To conduct simulation of the cavity behaviour during operation, a minimum system composed by the cavity, the piezoelectric tuner, and the klystron must be implemented in a numerical simulator. Due to the high computational costs of the mathematical models involved, real time cavity simulators are implemented in hardware using FPGA boards.
An important drawback of those implementation is a high knowledge barrier for their programming, requiring specialistic competences and specific instrumentation. In absence of a real-time requirements software based simulators offers a lower entry barrier, requiring only a general purpose personal computer, while allowing a shorter algorithm to implementation time. In the following sections simulations have been conducted using the SIMULINK model currently in use at the Laboratorio Acceleratori e Superconduttività Applicata (LASA) (Milan), offering a model of a TESLA cavity as employed at the LINACs in use in the European XFEL, where electronic beams are accelerated to 17.5 GeV before being sent to the undulators for

the generation of X-ray radiation.

In figure (23) an high level block scheme of the SIMULINK model,

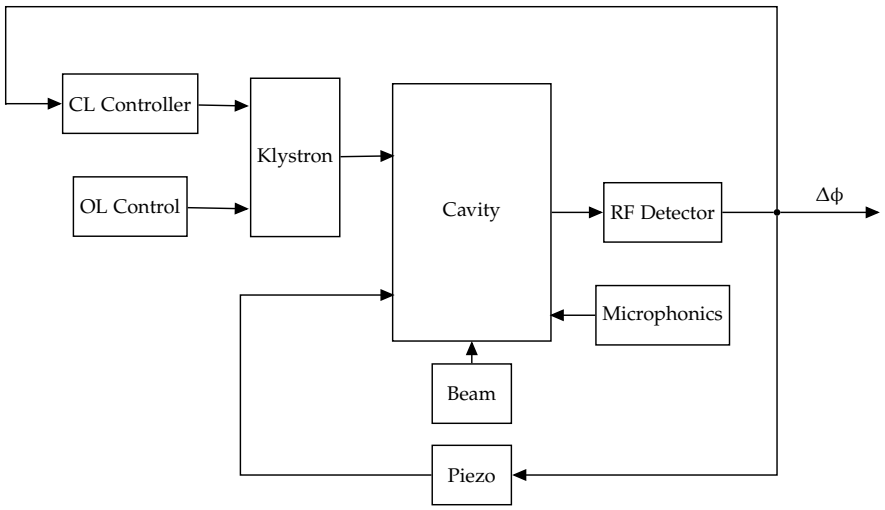

Figure 23: Block diagram of the TESLA SIMULINK model

completed with the added blocks for microphonic detuning simulation and mechanical compensation of detuning, is presented. The Low Level Radio Frequency (LLRF) control system, which includes the CL Controller, the Klystron and the RF detector, is responsible for the construction of the oscillating electromagnetic field inside the cavity, and its maintenance during the flat-top stage. In closed loop operation it compensates the effects of cavity detuning on the beam by increasing the Klystron power. The mechanical detuning compensation system is composed by the same RF detector plus the piezoelectric actuator completed by its controller.

Since the signal of the RF detector is used in both the control systems it must meet the more stringent requirements between the two. In particular its sampling rate is set by the needs of the LLRF control system, which has to deal with the dynamics of the resonant field, to 5μs, corresponding to a rate of 200kHz. To the internal detuning caused by Lorentz forces, modeled inside the cavity block, the contribution of microphonics its added as a disturbance from its relative block (24).

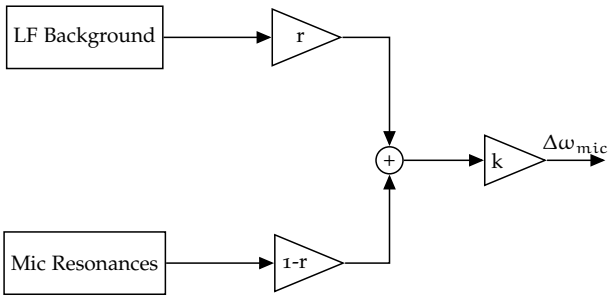

Figure 24: Block diagram of the microphonic subsystem.

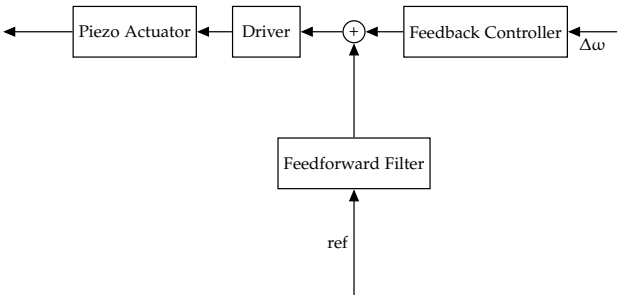

Figure 25: Block diagram of the piezo subsystem.

The low frequency background is simulated using a low pass filtered white-noise, while the microphonic resonances are modeled which sinusoidally oscillating signals superimposed to the background. The total noise rms and the ratio of the spectral power of the low frequency background to the resonances are controlled by the two adjustable parameter r and k.

5.2 CW OPERATION

During Continuous Wave (CW) operation the contribution from Lorentz forces to the cavity detuning remain manly a static term, (dynamics from fluctuation of the intensity of the oscillating electromagnetic field are negligible), that can be trivially compensate by pre-detuning the cavity accordingly and are therefore neglected in this section. In the proposed scheme (17), microphonics, the dominant cause of detuning in CW, are compensated by the feedback path where the controller is synthesized using the VRFT method.
In CW operation the cavity is kept at flat-top where the relationship (21) allows the recover of the detuning, minus a multiplicative constant, from the accelerating voltage measured by the RF detector without knowledge of the system parameters. As seen in 4 the system to be controlled is in general nonlinear, but the feedback control action of the LLRF system linearise the system seen by piezoelectric tuner, allowing the use of methods for the control of linear systems. By calling $S(z)$ the sensitivity of the closed loop system our only requirement is an attenuation of the microphonic disturbance $d(t)$. We can introduce a simple target sensitivity function with a single parameter ω_p representing the target frequency up to which microphonic detuning is to be attenuated by the control system.

$$S(z) = \frac{\omega_p}{s + \omega_p} \tag{77}$$

The VRFT method asks for the desired transfer function of the closed loop system. This is immediately obtained from the sensitivity function:

$$M(z) = 1 - S(z) \tag{78}$$

In the model reference cost function J_{MR} a frequency weighting term was also be introduced. Since we are interest in the attenuation of low frequency disturbances, $W(z)$ is given as a low pass filter:

$$W(z) = \frac{\omega_w}{s + \omega_w} \tag{79}$$

where ω_w is greater than ω_p. Among the class of feedback controllers linear in θ it has been chosen a PID due to the ease of implementation. It should be noted that due to approximation (51), the VRFT cost function is exactly equivalent to the model reference cost function only when the optimal controller belongs to the chosen class. We cannot expect this to be the case for a PID controller, it will be shown a posteriori that the error introduced is negligible for the chosen ω_p and the closed loop system obtained is close to the one requested.

$$C(z;\theta) = \vartheta_1 + \frac{z}{z-1}\vartheta_2 + \frac{z-1}{z}\vartheta_3 \tag{80}$$

$$\beta(z) = \begin{bmatrix} 1 & \frac{z}{z-1} & \frac{z-1}{z} \end{bmatrix}^T \tag{81}$$

A white noise was selected as the input to to the piezoelectric actuator to be certain to excite all the modes of the system in the frequency range of interest. Since this signal is going to detune the cavity, its rms (and therefore its peak values) should be chosen to not cause excessive detuning. If the Klystron is unable to keep the set accelerating voltage stable, the assumption made in the previous section about the linearity of the system does not hold. On the other hand, choosing a low rms increases the influence of noise during the synthesis experiments, requiring longer experiment durations. Considering a cavity bandwidth $\omega_{1/2}$ a detuning rms from the input signal of the piezoelectric of $\frac{1}{3}\omega_{1/2}$ has been chosen as a compromise.

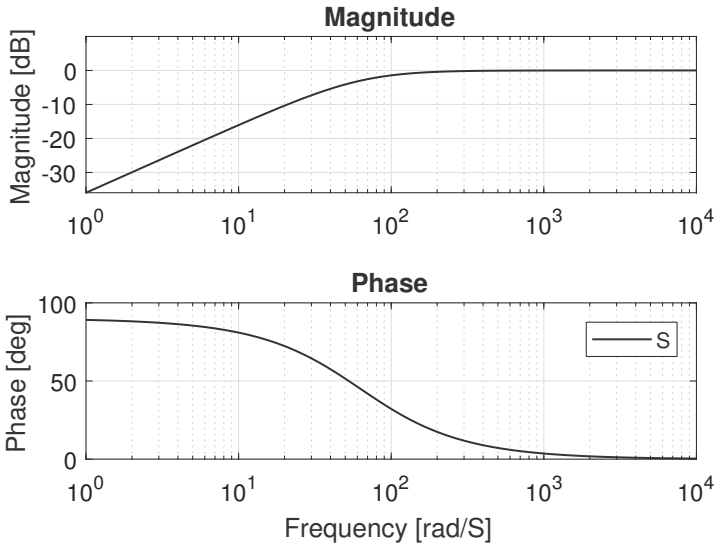

Figure 26: Target sensitivity function.

5.2.1 *Results*

In table (7) the simulation parameters used to show the main results obtained from the VRFT method are presented. To show the ability of

Parameter	Value	Description
ω_p	10Hz	Rejection bandwidth
ω_w	1kHz	Weighting bandwitdth
$\mathtt{beta}(z)$	$\left[1 \quad \frac{z}{z-1} \quad \frac{z-1}{z}\right]^T$	Controller Class
$\omega_{1/2}$	30Hz	Cavity bandwidth
$\mathtt{rms}(\Delta\omega_p)$	10Hz	Rms of experimental input
$\mathtt{rms}(\Delta\omega_{mic})$	5Hz	Rms of microphonic noise
t_{sim}	3.125s	Experiment duration

Table 7: VRFT Simulation Parameters

the synthesized feedback filter to compensate the microphonics' low frequency background a simulated microphonic sample was recorded and then fed to the cavity during CW operation with and without the feedback action. The results are shown in (27). The feedback filter is able to attenuate the low frequencies components below the higher frequency resonances. Critically the detuning from the resonances in the 10-100 Hz range is contained within a known amplitude range, while low frequency high detuning events, where the detuning is observed a full order of magnitude over its standards deviation, can occur stochastically during operation [17]. Since the klystron power required increased quadratically with the detuning (31), the feedback controller is able to prevent a failure of the klystron to sustain the accelerating voltage during these event even when the cavity is operated at very low bandwidths (which can be as low as 1Hz).

In (28) is show

The injected power from the klystron used to sustain the accelerating voltage is shown in figure (28) for a narrow cavity bandwidth, highlighting the effect of its quadratic dependence on detuning. The feedback controller is able to reduce the power required. Removing the low frequency backgrounds leaves the higher frequencies vibrations to cause oscillation of the detuning near the desired cavity resonant frequency. Thanks to the quadratic dependence on the power from the detuning the effects of those oscillations are attenuated in spite of the absence of actual mechanical compensation at those frequencies.

The VRFT method introduces an approximation in its cost function J_{VR} respect to the model reference cost function J_{MR}. The quality of the approximation in the minimum is greater the closer the minimizing parameter vector θ_0 brings the controller $C(z;\theta_0)$ to the ideal controller C_0, and therefore the obtained closed loop system $M(z;\theta_0)$

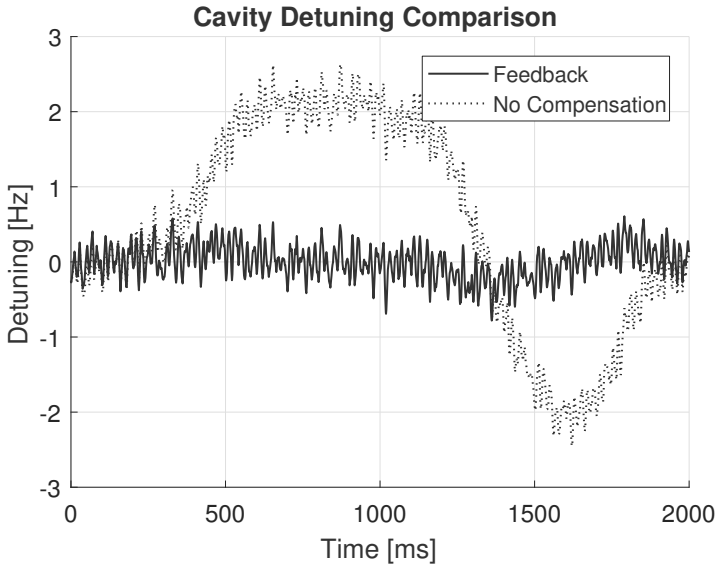

Figure 27: CW Cavity detuning.

closer to the desired model M_0. This ability of the parameter vector θ_0 depends on the model class chosen. We can now justify a posteriori the choice of the class of PID controllers by showing that the synthesized system is similar to the desired $M = 1 - S$. In (29), the feedback controller is switched on during a CW simulation, showing the behaviour of the simulated system with the synthesized controller C and the desired system M obtained from (77). There is no significant difference in their behaviour, J_{VR} is in its minimum a good approximation of J_{MR} and the PID is a good class in which to look for controllers. It should be noted that this may not hold if the requirements on S, and therefore M, change. In particular increasing the bandwidth of the feedback controller would erode the stability margin of the closed loop system; its behaviour, showing oscillation from the piezo resonances, would diverge from the desired M.

As seen in chapter 4 the use of an instrumental variable allows the VRFT method to remain consistent in the presence of noise. While asymptotically the cost function J_{VR} is unaffected by the disturbance, for an experiment of finite duration the noise will introduce an additive term to J_{VR} that leads to a non optimal controller (52). While there are no hard limits in principle for how long we could make the experiments lasts, it is generally desirable to keep the experiment short as long as the quality of the results is not significantly affected. To better characterize the effects of noise in typical conditions on the controller, it was chosen to conduct repeated simulations encompassing different data collection durations for a worse case noise rms of 5 Hz. The synthesized controllers were then tested in the operation of the closed loop system while affected by a known disturbance. For each controller the rms of the compensated detuning was collected and normalized with respect to the uncompensated detuning. In (30)

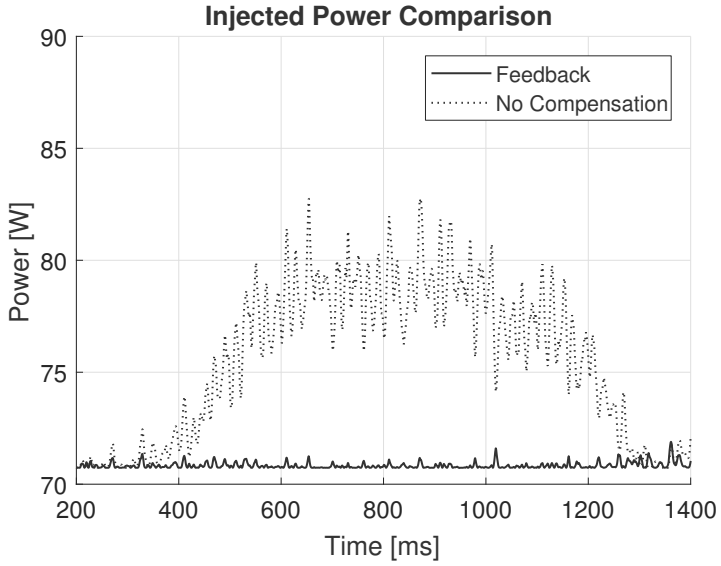

Figure 28: CW Cavity injected power.

the obtained data for constant rms noise is visualized using boxplots. The decrease of the influence of noise for longer experiment durations confirms the asymptotic insensitivity of the cost function J_{VR} when constructed using an instrumental variable. This also shows that only a few seconds of collected data are sufficient to produce a controller practically unaffected by noise. Since there are no particular constraints on the duration of the experiment, noise during synthesis is not an issue.
For a PID controller the influence a noise brings either a faster, with consequence loss of stability margin, or slower closed loop system. A comparison between two synthesized controller in presence of noise is shown in figure (31). Of the three $VRFT_1$ is the slowest and $VRFT_2$ is the faster with the ideal controller C_0 in the middle.

5.3 PULSED OPERATION

In pulsed operation the contribution of microphonics to the cavity detuning is much smaller (5Hz rms) compared to both the cavity bandwidth ($100 - 300$Hz) and the contribution of Lorentz forces (up to 600Hz) and therefore, while remaining a source of noise during synthesis experiments, their compensation has been neglected. In the proposed scheme (17) the effects of the Lorentz forces are compensated using a feedforward path where the filter is synthesized using the correlation approach.
The feedforward filter is going to take as input a reference signal such as to cancel the effects of the Lorentz forces on the cavity. Ideally the reference signal is going to be the detuning from the Lorentz forces itself with an opposite sign. The detuning itself is not measurable but

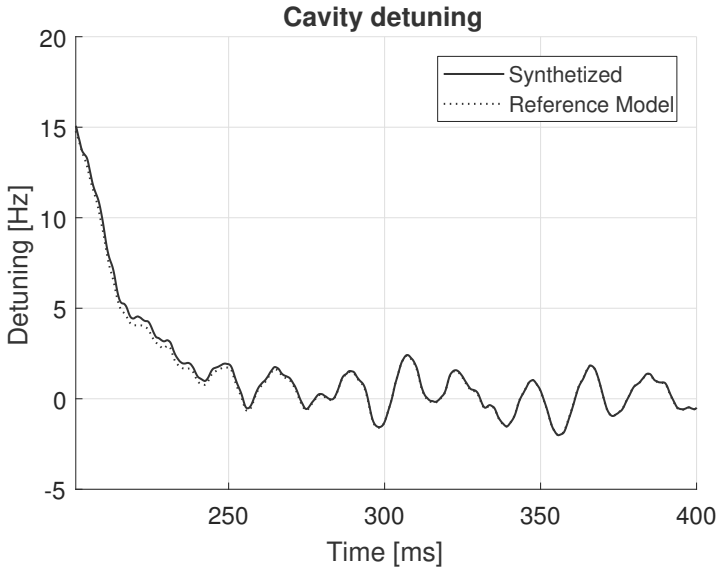

Figure 29: CW detuning of the closed loop system.

can either be obtained from simulations, or from the phase shift of the accelerating voltage. We can remember the relation (21) that allowed us for the feedback path to retrieve the detuning minus a multiplicative factor from the accelerating voltage (by taking the tangent of the phase shift) or to use the phase shift directly by introducing a small nonlinearity, both without knowledge of the cavity parameters. For these simulations the control signal is retrieved from the flat-top stage only, thus excluding a full compensation by feedforward action during the cavity fill. However the LINACs of the European XFEL spend a time interval of $500\mu s$ in the fill stage out of a total $1.3ms$. Limiting the feedforward action to the flat-top would leave a significant part of the pulse uncompensated. Furthermore this would introduce the necessity of bringing the resonant frequency to its desired value in a relative short time , approximately $100\mu s$, before the beam arrival, increasing the bandwidth requirements on the feedforward filter. Retrieving the detuning from the phase of the accelerating voltage is still possible using a non stationary solution for the RLC model of the cavity. Such approach has been successfully implemented, in hardware due to speed requirements, in [21]. While this solution allows a good reconstruction of the detuning during all operating phases of the cavity, it includes, in the form of the solution to the RLC equation, a model of the system complete with some cavity parameters. To keep the overall approach to detuning compensation direct, we can observe that for a reference signal, allowing a partial compensation during the fill stage, a perfect reconstruction of the detuning is not strictly needed. Therefore the use of a low-pass filtered extrapolation of the phase shift collected during flat-top is proposed.

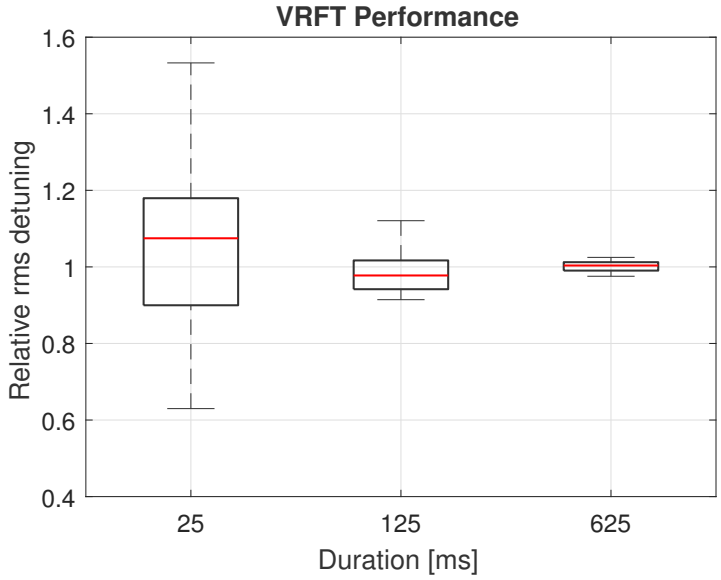

Figure 30: VRFT Performance across different experiment durations.

In figure (32) is shown such a reconstruction for a pulse. The main reason behind the low pass filter is due to avoid sharp steps that would pose a challenge to both the piezoelectric driver and the feedforward filter. It should be noted that the reconstructed Lorentz detuning is affected by microphonic noise that can either be neglected given the large bandwidth of the cavity ($100 - 300$Hz) compared to its rms (< 5Hz) or averaged across multiple reconstructions.
The input for the synthesis experiments needs also be constructed. According to equation (76) the spectrum of the experimental input acts as a weighting factor, together with the sensitivity function S of the closed loop system, to the cost function $J(\theta)$. The sensitivity function, realized by the VRFT method applied to the feedback path for the compensation of the microphonic detuning, is not known, since it contains the unknown plant P, but its modulus is approximately 1 for frequency higher than 10Hz, where the microphonic detuning is not compensated. Therefore the experimental input is the only weighting factor in the frequency domain in the range of interest for the compensation of Lorentz detuning. The use of the reference signal itself as experimental input allows to give more weight in the cost function to the frequencies that are actually going to be excited by the reference signal itself during use. This also limits the reconstruction in the frequency domain causing the loss spectral information at higher frequencies. This could lead to poorly conditioned matrices in the numerical algorithm for the solution of the least squares formula. The problem was overcome by limiting the sampling frequency of the filter, and therefore restricting the frequency range considered by the cost function.
The signal to the feedforward filter is downsampled to 20kHz to dis-

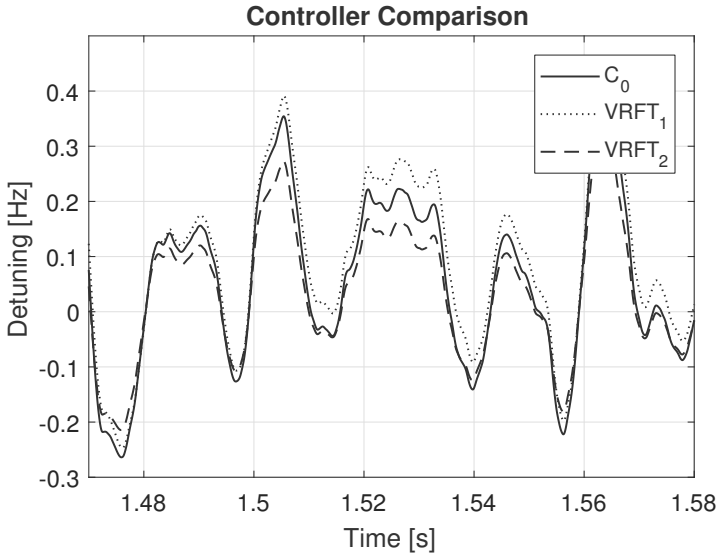

Figure 31: Comparison between noise affected controllers.

card in the numerical solution frequencies poorly excited by the experimental input, that would lead to a poorly conditioned matrix. This has also the effect of reducing the order of the filter required to capture the oscillating dynamics of the piezoelectric actuator. This limit does lead to discard data since the full 200kHz signal can still be used to synthesized the 20kHz filter.
The choice of the rms of the input signal, as for the VRFT experiment, is going to be a compromise. The experimental input is applied as a disturbance on the control signal of the piezoelectric driver causing a detuning of the cavity. A high rms could cause excessive detuning, causing a failing of the Klystron to maintain the accelerating voltage constant during flat-top while a low rms increase the influence of the microphonic noise on the synthesized controller. Since in pulsed operation cavities are operated with a higher bandwidth ($100 - 300$Hz) compared to CW operation ($1 - 30$) while the microphonics rms does not increase it was chosen a detuning rms from the input signal of the piezoelectric of $\frac{1}{10}\omega_{1/2}$.
The correlation approach as presented in chapter 4 needs to look for the optimal filter in the class of filters linear in their parameter vector, the use of a Finite Impulse Response (FIR) filter is proposed:

$$\begin{aligned} F(z;\theta) &= \beta^T(z)\theta \\ \beta(z) &= \begin{bmatrix} 1 & z^{-1} & z^{-2} & \dots & z^{-n} \end{bmatrix}^T \end{aligned} \tag{82}$$

Since this approach to the synthesis of the filter does not provide a way to choose the order of the filter a priori, the order choice will be justified later by a cross-validation procedure. Filters of different orders will be compared in terms of rms detuning during flat-top operation and $n = 20$ will be shown to minimize the detuning.

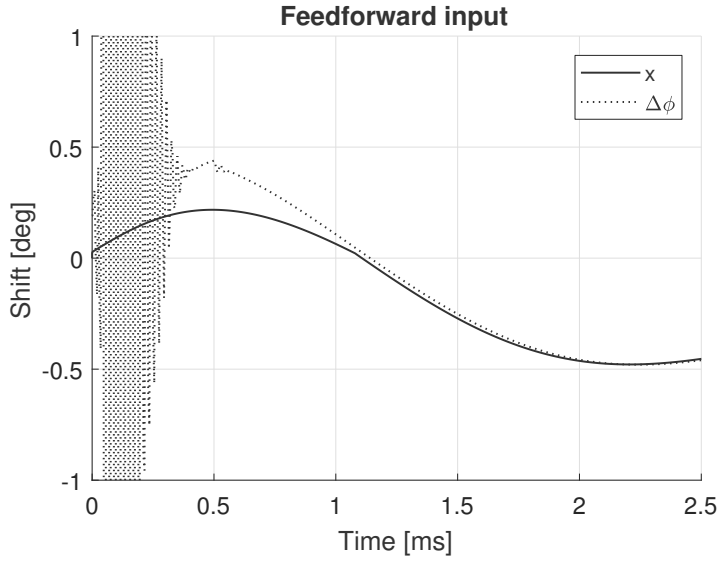

Figure 32: Construction of the feedforward reference signal

5.3.1 *Results*

Parameter	Value	Description
f_s	20kHz	Sampling Frequency
$\beta(z)$	$\begin{bmatrix} 1 & z^{-1} & \dots & z^{-50} \end{bmatrix}^T$	Filter Class
n	20	Filter Order
$\omega_{1/2}$	250Hz	Cavity bandwith
$\Delta\omega$	250Hz	Pre-Detuning
$\mathrm{rms}(P(z)x(t))$	25Hz	Rms of experimental input
$\mathrm{rms}(\Delta\omega_{mic})$	5Hz	Rms of microphonic noise
t_p	3ms	Pulse duration
$t_{flat-top}$	0.8ms	Flat-top duration
t_{sim}	125ms	Synthesis Experiment duration

Table 8: Correlation Approach Simulation Parameters

The simulation parameters used in simulation are presented in table 8. To show the ability of the feedforward filter to compensate the detuning due to Lorentz forces during pulsed operation a comparison between a compensated and uncompensated pulse is shown in figure (33). The reference signal constructed as in (32), fed into the feedforward filter synthesized using the correlation approach, is able to compensate most of the detuning during the flat-top stage. At the beginning of the decay stage of operation the control input of the piezo is switched off leaving it to return to the equilibrium position by the free motion of the tuner-cavity system. This is the cause of the

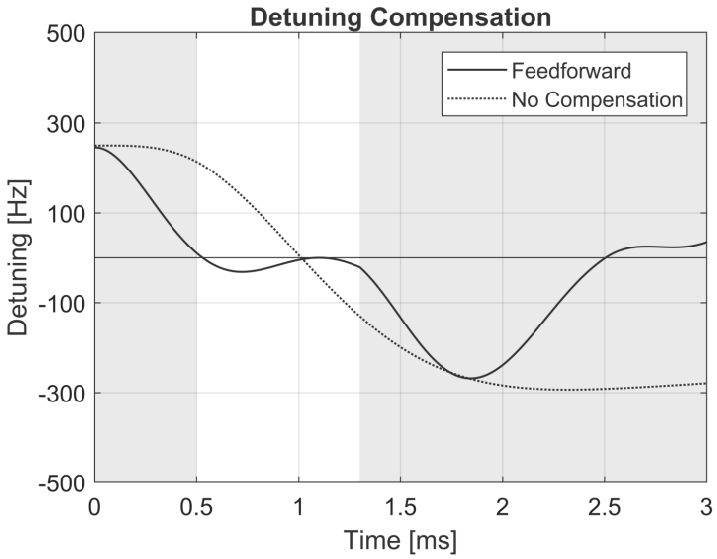

Figure 33: Pulsed Cavity detuning.

visible ringing of the cavity resonant frequency after the 1.3ms mark. If the ringing were to persist until the next pulse (100ms) it would introduce a further detuning term. Extending the reference signal in the decay stage to bring the piezoelectric actuator in a controlled manner to zero displacement (for example by adding a decaying term to its last value in the flat-top region) is expected to be a viable strategy to reduced the ringing should the need arise. The rms for the detuning in the compensated case is 25Hz compared to 120Hz for the uncompensated pulse. This translate to a mean injected power of 240*W* during the flat-top stage instead of 270*W*, as shown in figure (34).

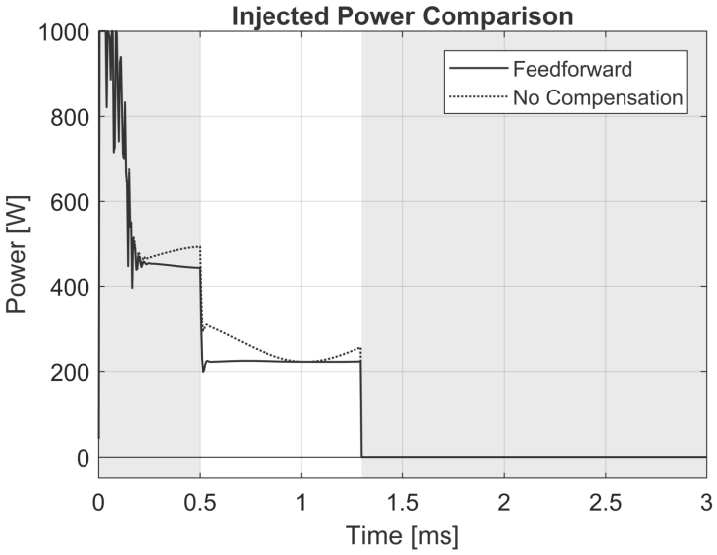

Figure 34: Pulsed Cavity injected power.

In figure (35) is also show the power injected by the klystron during pulsed operation with the addition of an accelerating beam of $2mA$. The cavity pre-detuning has been chosen to obtain a detuning of the cavity close to zero during pulse propagation (from $0.9ms$ to $1.1ms$) even without the dynamic compensation of the piezoelectric actuator. The power savings obtained by the feedforward filter are therefore realized mostly during the approaching of the desired accelerating voltage in the fill stage ($0.3 - 0.5ms$) and in the maintenance of the resonating field during the flat-top stage and not in the acceleration of the beam itself.

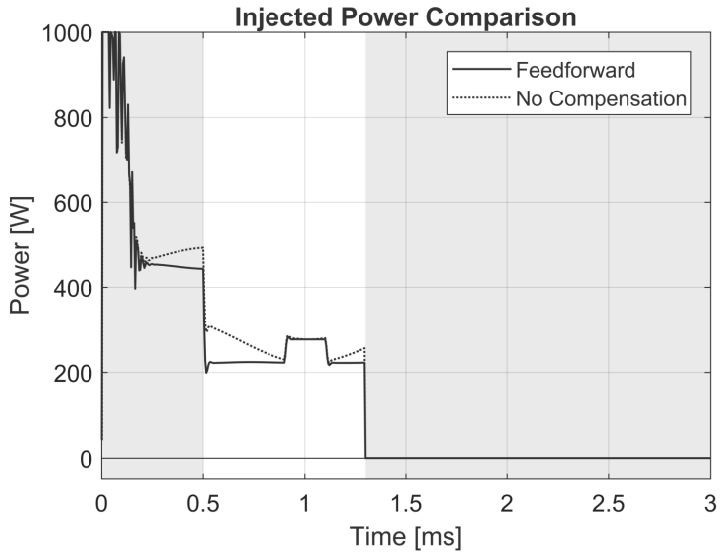

Figure 35: Pulsed Cavity injected power with beam acceleration.

The choice of filter of order 20 was made with no a priori justification. In figure (36) filters obtained from the same simulated experiment but of different order are compared following a cross-validation procedure where their quality is given by the rms detuning during flat-top operation. The orders $20 - 25$ corresponds to a minimum of the detuning during the flat-top stage. It can be observed that 25 samples correspond to a time window of $1.3ms$ exactly the duration of the pulse. While adding further samples to the filter, increasing its order, may potentially lead to a better tracking over a longer time interval, adding filter coefficients that are not utilized leads to a decrease of the filter performance in the short (compared to the step response of the piezo actuator, that could take 100 ms or more to reach steady-state like conditions) time interval of the pulse.

As seen in chapter 4 the correlation approach is asymptotically unaffected by noise provided that its expected value is zero. For an experiment of limited duration the correlation cost function $J(\theta)$ is affected by noise and its minimization will yield a non optimal parameter vector θ, different from the one minimizing the correlation

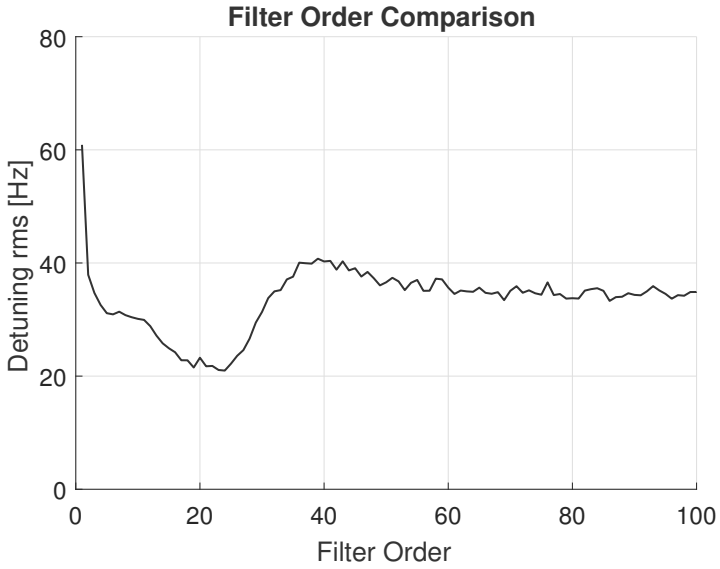

Figure 36: Pulsed Cavity detuning at different filter orders.

from the reference signal to the output. To characterize the influence of microphonics on the correlation approach in terms of its synthesized filter it was chosen to conduct repeated simulated synthesis experiments at different noise levels. Each synthesized filter is then tested in the compensation of the Lorentz detuning during a pulse and the resulting rms during flat-top is collected. To reduce the computational time required a duration of 25ms is considered instead of 125ms. The result is presented in figure (37). Microphonic noise during synthesis introduces variations on the quality of the obtained filters, leading to a worse compensation of the Lorentz detuning at increasing levels of noise.

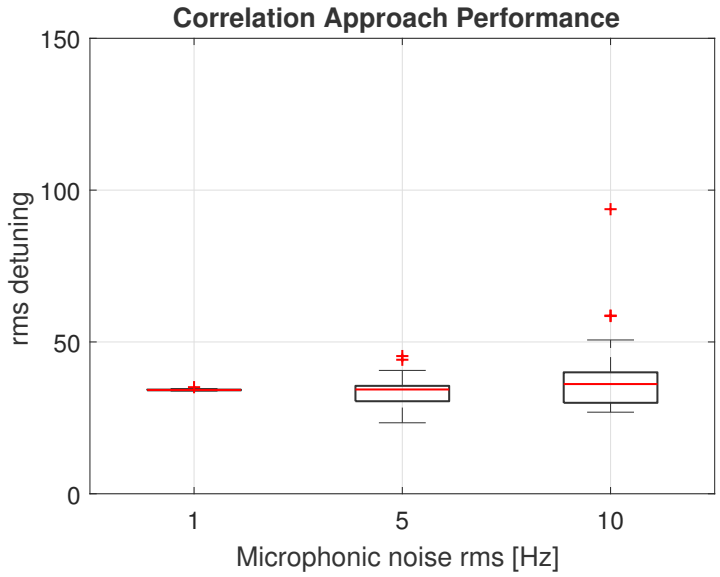

Figure 37: Correlation Approach Performance

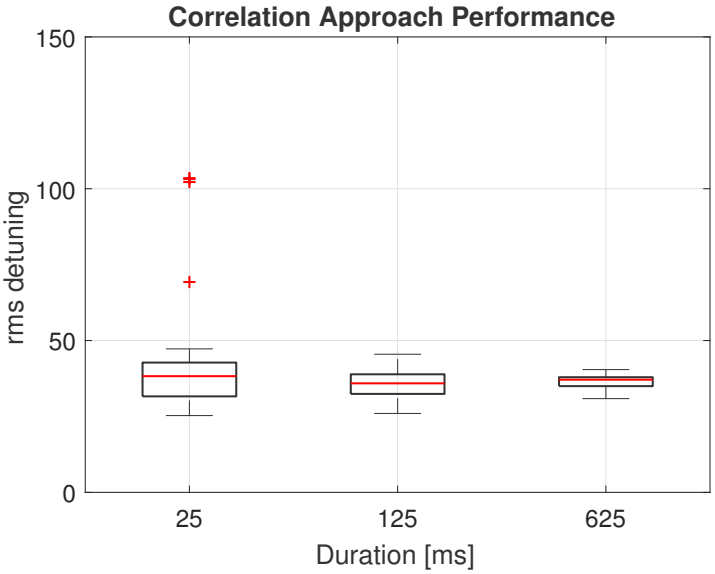

Figure 38: Correlation Approach Performance across different experiment durations.

The amplitude of the input signal during the synthesis or the duration of the experiment can both be increased to reduce the noise influence on the correlation cost function. In order to show the consistency of the correlation approach in the presence of microphonic noise, repeated simulated synthesis experiments were conducted. The resulting feedforward filter were then applied to the compensation of a test pulse. The results are presented in figure (38). Since the filter is tested on a single pulse the microphonic noise is not compensated, contributing to the variance of the detuning rms even at higher experimental durations. Once this effect has been taken into account the results confirms the asymptotic insensitivity of the cost function to microphonic noise. Since both the VRFT applied to the synthesis of the feedback filter and the correlation approach applied to the synthesis of the feedforward filter are consistent, the overall method for the compensation of microphonic detuning is consistent.

6

CONCLUSIONS

The high accelerating gradients of the resonant electromagnetic field, external vibrations and pressure fluctuation causes deformation of the accelerating cavities of the LINACs employed in the generation of X-ray radiation in XFEL facilities. To address the loss of efficiency and beam quality, caused by the cavity detuning from these deformations, devices capable of mechanical compensation are adopted. The complex mechanical coupling of the piezoelectric actuator responsible for compensating the detuning during operation has led to the use of control schemes with feedforward action or combined feedforward/feedback action and direct iterative control methods. The controlled system obtained is nonlinear: its stability and ability to converge to feedforward filters capable of compensation depends on the initial conditions and manually tuned parameters of the iteration algorithm.
This thesis aims at reducing the complexity of the control system by proposing the use of non-iterative direct control methods. The controller is computed offline using data collected from input/output experiments yielding an overall linear device with no convergence issues. On a simulated system, the VRFT method has shown its ability to synthesize a feedback controller capable of compensating the low frequency microphonic background, allowing the continuous wave operation of XFELs at low cavity bandwidths (possibly down to 5 Hz), while the detuning from Lorentz forces was compensated in pulsed operation by a feedforward filter synthesized on the basis of the correlation approach. Power savings were achieved for both pulsed and continuous wave operations and characterized for typical cavity conditions. Repeated experiments in the presence of noise have shown the consistency of both methods and their ability to provide controllers or filters nearly unaffected by the microphonic noise.

6.1 FURTHER DEVELOPMENTS

Iterative methods adjust the parameters of the filter or controller at each iteration, responding during operation to changes in the system, such as the increase of the piezoelectric temperature. The performance loss over time of the feedback controller and feedforward filter from non-iterative methods remains to be characterized on a real system, and it could represent a decisive factor on the feasibility on the proposed control approach.
The use of a PID class for the feedback controller in the VRFT method

represent a conservative choice. System stability respects the Bode criterion and the low compensation bandwidth keeps the tuner-cavity resonances below the instability threshold. However this low bandwidth does not allow compensation of the mechanical vibrations responsible for the resonances in the microphonic spectrum. The use of a high order class for the controller in the VRFT algorithm, one capable to include in the feedback action these resonances, remains to be investigated. Compensation limited by the actuator resolution could be achieved, making possible the use of very low (1 Hz) cavity bandwidths in continuous wave operation.

BIBLIOGRAPHY

[1] Massimo Altarelli et al. *The European X-Ray Free-Electron Laser, Technical design report*. Tech. rep. 2006.

[2] B. Aune et al. *The Superconducting TESLA Cavities*. 2000.

[3] Angelo Bosotti. "Piezo ceramics for LLRF". In: 2007.

[4] Angelo Bosotti et al., eds. *Full Characterization of the Piezo Blade Tuner for Superconductive RF Cavities*. INFN/LASA, Segrate (MI), BESSY GmbH, Berlin, and DESY, Hamburg. 2008.

[5] J. Branlard, V. Ayvazyan, M. Grecki, H. Schlarb, C. Schmidt, W. Cichalewski, K. Gnidzinska, A. Piotrowski, K. Przygoda, and W. Jałmuzna, eds. *LLRF Tests of XFEL Cyromodules at AMTF: First Experimental Results*. 2013.

[6] R. Brinkman, E.A. Schneidmiller, J. Sekutowicz, and M.V. Yurkov. "Prospects for CW and LP operation of the European XFEL in hard X-ray regime". In: (2014).

[7] M.C. Campi, A. Lecchini, and S.M. Savaresi. "Virtual reference feedback tuning: a direct method for the design offeedback controllers". In: *Automatica* (2002).

[8] W. Cichalewski, A. Napieralsk, J. Branlard, and C. Schmidt, eds. *European XFEL Cavities Piezoelectric Tuners Control Range Optimization*.

[9] J. R. Delayen and G. K. Davis, eds. *Piezoelectric Tuner Compensation of Lorentz Detuning in Superconductive Cavities*. Jefferson Lab. 2013.

[10] M. Fouaidy, G. Martinet, N. Hammoudi, F. Chatelet, A. Olivier, S. Blivet, H. Saugnac, and A. Le Goff. "Electromechanical, Thermal Properties and Radiation Hardness Tests of Piezoelectric Actuators at Low Temperature". In: 2003.

[11] Arne Hessenbrunch. "A brief history of x-rays". In: *Endeavour* (2003).

[12] Alireza Karimi, Mark Butcher, and Roland Longchamp. "Model-Free Precompensator Tuning Based on the Correlation Approach". In: *IEEE Transactions on Control Systems Technology* (2008).

[13] Oliver Kugeler, Wolfgang Anders, Jens Knobloch, and Axel Neumann. "Characterisation of Microphonics in HoBiCaT". In: 2006.

[14] Matthias U. Liepe. "Superconducting Multicell Cavities for Linear Colliders". PhD thesis. Universitat Hamburg, 2001.

[15] Lutz Lilje. *Fabrication and Quality Control of the Frequency Tuner for the XFEL*. ECFA LC2013 Workshop. 2013.

[16] A. Neumann, W. Anders, O. Kugeler, and J. Knobloch. "Analysis and active compensation of microphonics in continuous wave narrow-bandwidth superconducting cavities". In: (2010).

[17] Axel Neumann. "Compensating Microphonics in SRF Cavities to Ensure Beam Stability for Future Free-Electron-Lasers". PhD thesis. Humboldt University of Berlin, 2008.

[18] Claudio Pellegrini and Joachim Stöhr. *X-Ray Free Electron Lasers: Principles, Properties and Applications*.

[19] Y. Pischalnikov, B. Hartman, J. Holzbauer, W. Schappert, S. Smith, and J.C. Yun, eds. *Reliability of the LCLS II SRF Cavity Tuner*. 2015.

[20] K. Przygoda, J. Branlard, O. Hensler, H. Schlarb, C. Schmidt, K. Kasprzak, W. Cichalewski, and T. Pozniak, eds. *Testing Procedures For Fast Frequency Tuners of XFEL Cavities*. 2015.

[21] Konrad Przygoda. "Development of Control System for Fast Frequency Tuners of Superconducting Resonant Cavities for FLASH and XFEL Experiments". PhD thesis. Technical University of Łódź, 2010.

[22] J. Sekutowicz. *Superconducting Linear Accelerator for the European XFEL*. International Workshop on X-ray Diagnostics and Scientific Application of the European XFEL. 2010.

[23] *TESLA XFEL: First Stage of the X-Ray Laser Laboratory*. Tech. rep. DESY, 2002.

[24] Kenji Uchino. *Introduction to Piezoelectric Actuators and Transducers*. Tech. rep. International Center for Actuators and Transducers, Penn State University, 2003.

[25] Masashi YAMANAKA. *ILC tuner development at KEK*. Mechanical Engineering Center, KEK. 2016.